



*The Abdus Salam
International Centre for Theoretical Physics*



2223-5

Winter College on Optics in Imaging Science

31 January – 11 February, 2011

Computational Imaging

L. Yaroslavsky
*Tel Aviv University
Israel*

Imaging Optics and Computational Imaging

Leonid P. Yaroslavsky

**School of Electrical Engineering,
Dept. of Physical Electronics, Tel Aviv
University,
Tel Aviv, Israel**

**ICTP Winter College on Optics in Imaging
Science, Trieste, Italy, Febr. 2011**

❑ Introduction

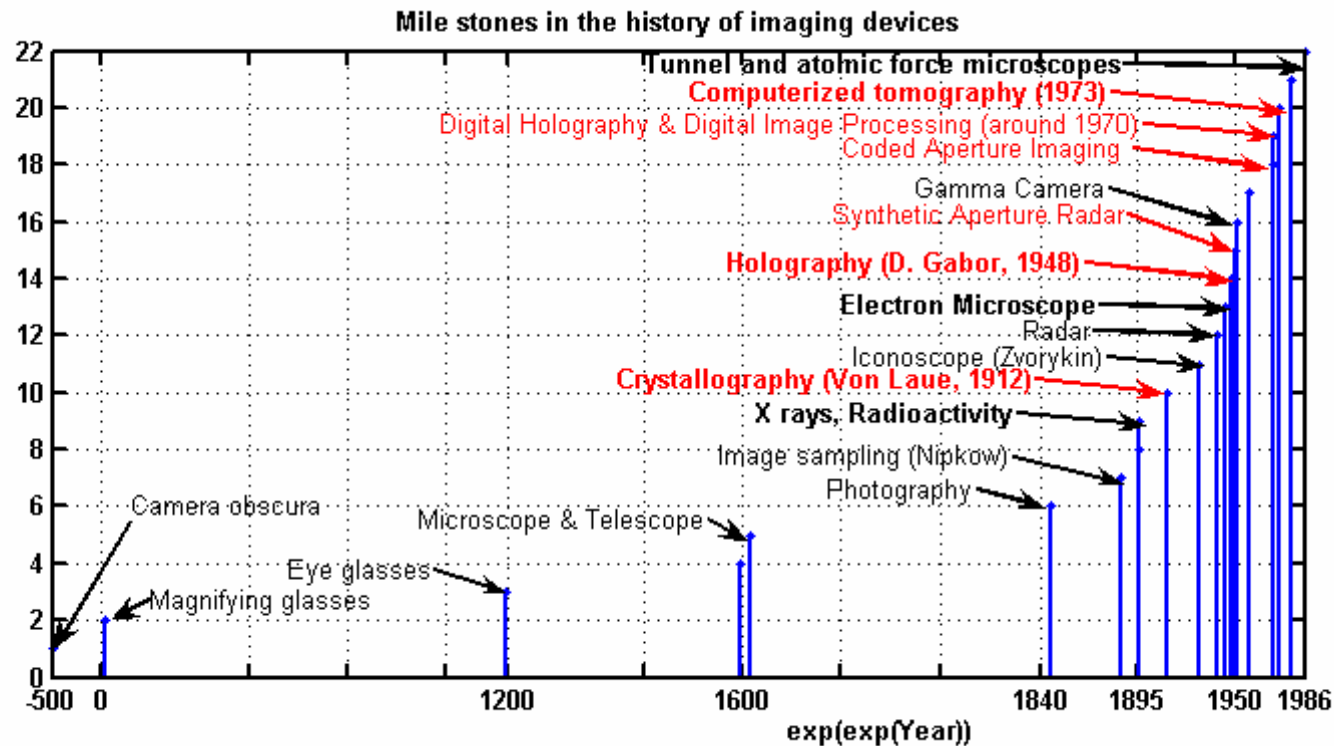
❑ Linking optical and digital image processing

- Principles of discrete representation of signal transformations
- Discrete representations of imaging transforms

❑ Examples of computational imaging :

- Stabilization and super-resolution in turbulent video
- Image recovery from sparse sampling:
 - Discrete sampling theorem
 - Signal recovery as an approximation task
 - “Compressing sensing” approach
- Imaging without optics: Optics less smart sensors

❑ Conclusion: computational imaging and evolution of vision in nature



Imaging has always been the primary goal of informational optics. The whole history of optics is a history of creating and perfecting imaging devices. The main characteristic feature of the latest stage of the evolution of informational optics is integrating of physical optics with digital computers. With this, informational optics is reaching its maturity. It is becoming digital and imaging is becoming computational.

Image processing capability of optics:

- Image formation from light wave-front**
- Image geometrical transformations**
- Image transforms (Fourier & Fresnel)**
- Image correlation and convolution with template**
- Image brightness point-wise manipulation (electro-optics)**

New qualities brought in to imaging systems by digital computers

- Flexibility and adaptability: no hardware modifications are necessary to reprogram digital computers to solving different tasks.**
- Digital computers integrated into optical imaging systems enable them to perform any operations needed and not only element-wise and integral signal transformations, such as spatial and temporal Fourier analysis, signal convolution and correlation that are characteristic for analog optics. This removes the major limitation of analog optical information processing.**
- Acquiring and processing quantitative data contained in optical signals and connecting optical systems with other informational systems and networks is most natural when data are handled in a digital form.**

Digital vs analog imaging: a tradeoff between good and bad features.

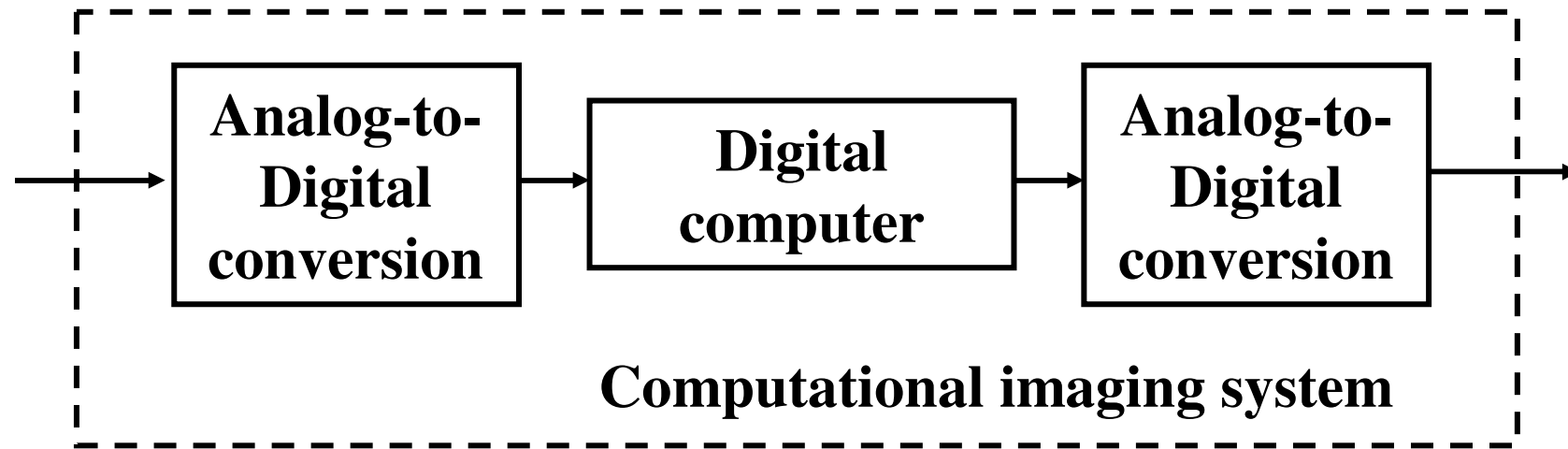
The fundamental limitation of digital signal processing is the speed of computations. What optics does in parallel and with the speed of light, computers perform as a sequence of very simple logical operations with binary digits, which is fundamentally slower whatever the speed of these operations is.

Optimal design of image systems requires appropriate combination of analog and digital processing using advantages and taking into consideration limitations of both.

Linking optical and digital image processing

Marriage analog electro-optical and digital processing requires appropriate linking analog and digital signals and transformations.

The consistency and mutual correspondence principle

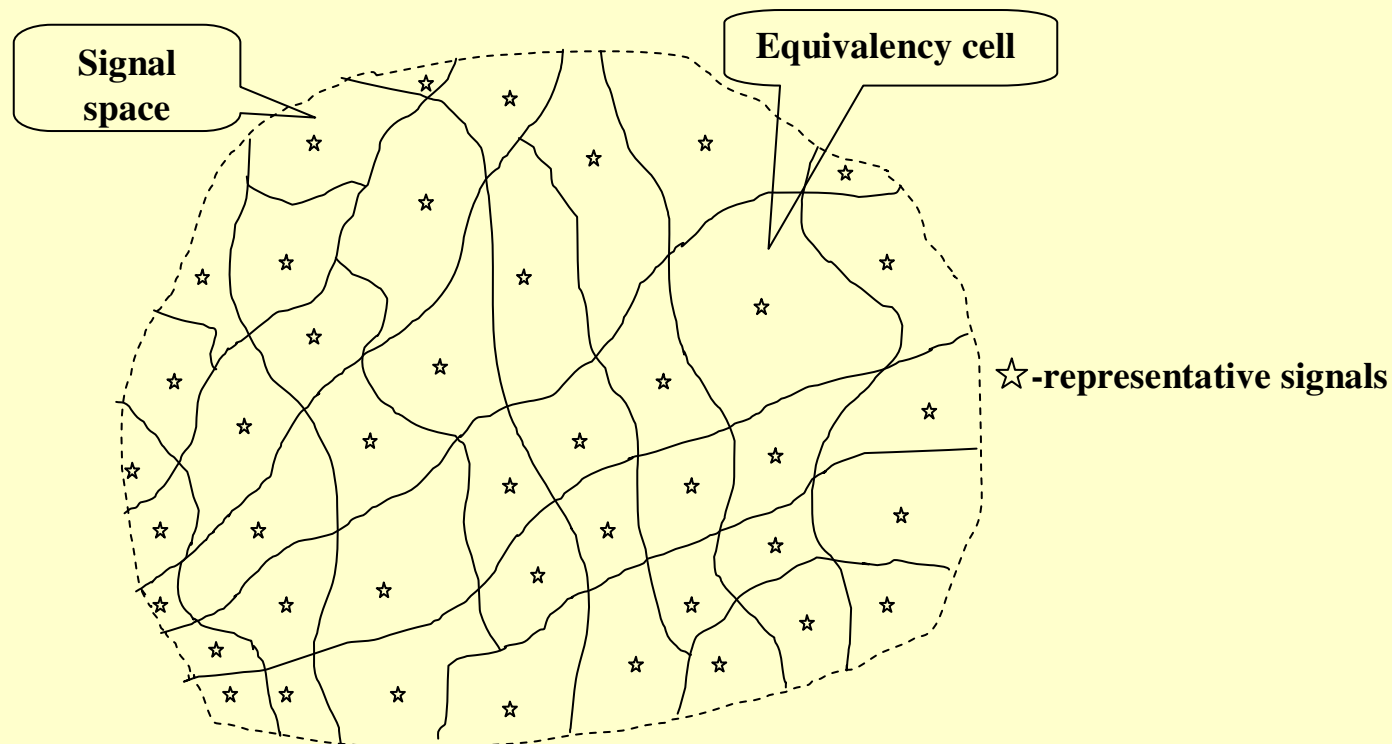


- Digital processors incorporated into optical information systems should be regarded and treated together with signal discretization and reconstruction devices as integrated analog units and should be specified and characterized in terms of equivalent analog transformations.
- Discrete transformation corresponds to its analog prototype if both act to transform identical input signals into identical output signals.
- Discrete representation of signal transformations should parallel that of signals.

SIGNAL DIGITIZATION

General quantization:

- Splitting signal space into equivalence cells
- Mapping signal space into a set of natural numbers
- Associating each number with a “representative” signal of the corresponding equivalence cell



SIGNAL DIGITIZATION:

Two step digitization:

➤ Signal discretization by means of signal expansion over a set of basis functions

$$a(x) = \sum_{k=0}^{N-1} \alpha_k \varphi_k^{(r)}(x)$$

Signal
reconstruction
basis functions

$$\alpha_k = \int_X a(x) \varphi_k^{(d)}(x)$$

Signal
discretization
basis functions

➤ Element-wise quantization of the representation coefficients $\{\alpha_k\}$

Signal discretization

Types of discretization basis functions:

- Shift (sampling) basis functions $\{\{\varphi^{(s)}(x - k\Delta x)\}; \{\varphi^{(r)}(x - k\Delta x)\}\}$
- Scaled basis functions $\{\{\varphi^{(d)}(kx)\}; \{\varphi^{(r)}(kx)\}\}$
- Shift&Scale basis functions: Wavelets

The sampling theorem

The sampling theorem formulated in terms of the accuracy of reconstruction of continuous signals from their samples:

- The least square error approximation $\tilde{a}(x)$ of signal $a(x)$ from its samples $\{a_k\}$ taken on a uniform sampling grid with sampling interval Δx is

$$\tilde{a}(x) = \sum_{k=-\infty}^{\infty} a_k \operatorname{sinc}[2\pi(x - k\Delta x)/\Delta x],$$

provided that signal samples $\{a_k\}$ are obtained as:

$$a_k = \frac{1}{\Delta x} \int_{-\infty}^{\infty} a(x) \operatorname{sinc}[2\pi(x - k\Delta x)/\Delta x] dx$$

- The approximation mean square error is minimal in this case and is equal to:

$$\int_{-\infty}^{\infty} |a(x) - \tilde{a}(x)|^2 dx = \int_{-\infty}^{-1/\Delta x} |\alpha(f)|^2 df + \int_{1/\Delta x}^{\infty} |\alpha(f)|^2 df = 2 \int_{1/\Delta x}^{\infty} |\alpha(f)|^2 df$$

where $\alpha(f) = \int_{-\infty}^{\infty} a(x) \exp(i2\pi fx) dx$ is signal Fourier spectrum and f is frequency, and

$\operatorname{sinc}(x) = \sin x / x$ is “Sinc-function”, the point-spread function of the ideal low-pass filter

$$\operatorname{sinc}(2\pi x / \Delta x) = \Delta x \int_{-1/\Delta x}^{1/\Delta x} \exp(-i2\pi fx) df$$

Discrete representation of integral transforms

Discrete representation of convolution integral

The convolution integral of a signal $a(x)$ with shift invariant kernel $h(x)$:	$b(x) = \int_{-\infty}^{\infty} a(\xi)h(x - \xi)d\xi$
Digital filter for samples $\{a_k\}$ and $\{b_k\}$ of input and output signals	$b_k = \sum_{n=0}^{N_h-1} h_n a_{k-n}$ <p>N_h is the number of non-zero samples of h_n</p>
Discrete impulse response $\{h_n\}$ of the digital filter for input and output signal sampling bases $\phi_0^{(s)}(x)$ and $\phi_0^{(r)}(x)$ and sampling interval Δx	$h_n = \int_{-\infty}^{\infty} \int_{-\infty}^{\infty} h[x - \xi - n\Delta x] \phi^{(r)}(\xi) \phi^{(s)}(x) dx d\xi,$
Overall point spread function of an analog filter equivalent to a given digital filter	$h_{eq}(x, \xi) = \sum_{k=0}^{N_b-1} \sum_{m=0}^{N_h-1} h_n \phi^{(r)}(x - n\Delta x) \phi^{(s)}[\xi - (k - n)\Delta x]$ <p>N_b is the number of samples of the filter output signal $\{b_k\}$ involved in reconstruction of analog output signal $b(x)$, N_h is the number of samples of the digital filter PSF and Δx is the signal sampling interval</p>
Overall frequency response $H_{eq}(f, p)$	$H_{eq}(f, p) = \int_{-\infty}^{\infty} \int_{-\infty}^{\infty} h_{eq}(x, \xi) \exp[i2\pi(fx - p\xi)] dx d\xi = SV(f, p) CFrR(p) \Phi^{(r)}(f) \Phi^{(s)}(p).$ $SV(f, p) = \sum_{k=0}^{N_b-1} \exp[i2\pi(f - p)k\Delta x]; CFrR(p) = \sum_{n=0}^{N_h-1} h_n \exp(i2\pi n\Delta x)$ $\Phi^{(r)}(f) = \int_{-\infty}^{\infty} \phi^{(r)}(x) \exp(i2\pi fx) dx; \Phi^{(s)}(p) = \int_{-\infty}^{\infty} \phi^{(s)}(x) \exp(i2\pi px) dx;$

Discrete representation of 1D Fourier integral transform

<i>1-D direct and inverse integral Fourier Transforms of a signal $a(x)$</i>	
$\alpha(f) = \int_{-\infty}^{\infty} a(x) \exp(i2\pi fx) dx$	$a(x) = \int_{-\infty}^{\infty} \alpha(f) \exp(-i2\pi fx) df$
<i>Direct and Inverse Canonical Discrete Fourier Transforms (DFT)</i>	
$\alpha_r = \frac{1}{\sqrt{N}} \sum_{k=0}^{N-1} a_k \exp\left(i2\pi \frac{kr}{N}\right)$	$a_k = \frac{1}{\sqrt{N}} \sum_{r=0}^{N-1} \alpha_r \exp\left(-i2\pi \frac{kr}{N}\right)$
<i>Direct and Inverse Shifted DFTs (SDFT(u, v)):</i>	
<u>Sampling conditions:</u> - Signal and signal sampling device coordinate systems as well as, correspondingly, those of signal spectrum and of the assumed signal spectrum discretization device, are shifted with respect to each other in such a way that signal sample $\{a_0\}$ and, correspondingly, sample $\{\alpha_0\}$ of its Fourier spectrum are taken in signal and spectrum coordinates at points $x = -u\Delta x$ and $f = -v\Delta f$. Signal “cardinal” sampling: $\Delta x = 1/N\Delta f$	
$\alpha_r^{u,v} = \frac{1}{\sqrt{N}} \sum_{k=0}^{N-1} a_k \exp\left[i2\pi \frac{(k+u)(r+v)}{N}\right]$	$a_k = \frac{1}{\sqrt{N}} \sum_{r=0}^{N-1} \alpha_r^{u,v} \exp\left[-i2\pi \frac{(k+u)(r+v)}{N}\right]$
<i>Direct and Inverse Discrete Cosine Transform (DCT):</i>	
<u>Sampling conditions:</u> - Special case of SDFT for sampling grid shift parameters: $u = 1/2; v = 0$ Analog signal of final length is, before sampling, artificially padded with its mirror copy to form a symmetrical sampled signal of double length: $\{a_k = a_{2N-1-k}\}$;	
$\alpha_r = \frac{2}{\sqrt{2N}} \sum_{k=0}^{N-1} a_k \cos\left(\pi \frac{k+1/2}{N} r\right)$	$a_k = \frac{1}{\sqrt{2N}} \left[\alpha_0 + 2 \sum_{r=1}^{N-1} \alpha_r \cos\left(\pi \frac{k+1/2}{N} r\right) \right]$
<i>Direct and Inverse Scaled Shifted DFTs (ScSDFT($u, v; \sigma$))</i>	
<u>Sampling conditions:</u> - Sampling rate is σ times the cardinal rate: $\Delta x = 1/\sigma N\Delta f$ - Sampling shift parameters: $u, v \neq 0$	
$\alpha_r^\sigma = \sum_{k=0}^{N-1} a_k \exp\left[i2\pi \frac{(k+u)(r+v)}{\sigma N}\right]$	$a_k = \sum_{r=0}^{\sigma N-1} \alpha_r^\sigma \exp\left[-i2\pi \frac{(k+u)(r+v)}{\sigma N}\right]$

Discrete representation of 2D Fourier integral transform

2-D direct and inverse integral Fourier Transforms of a signal $a(x, y)$

$$\alpha(f, p) = \int_{-\infty-\infty}^{\infty} \int_{-\infty-\infty}^{\infty} a(x, y) \exp[i2\pi(fx + py)] dx dy$$

$$a(x, y) = \int_{-\infty-\infty}^{\infty} \int_{-\infty-\infty}^{\infty} \alpha(f, p) \exp[-i2\pi(fx + py)] df dp$$

2-D separable direct and inverse canonical DFTs:

Sampling conditions:

- Sampling in a rectangular sampling grid with cardinal sampling rates $\Delta x = 1/N_1 \Delta f_x$, $\Delta y = 1/N_2 \Delta f_y$
- Zero sampling grid shift parameters

$$a_{k,l} = \frac{1}{\sqrt{N_1 N_2}} \sum_{k=0}^{N_1-1} \sum_{l=0}^{N_2-1} \alpha_{r,s} \exp \left[-i2\pi \left(\frac{kr}{N_1} + \frac{ls}{N_2} \right) \right]$$

$$a_{k,l} = \frac{1}{\sqrt{N_1 N_2}} \sum_{k=0}^{N_1-1} \sum_{l=0}^{N_2-1} \alpha_{r,s} \exp \left[-i2\pi \left(\frac{kr}{N_1} + \frac{ls}{N_2} \right) \right]$$

Scaled Shifted DFTs

Sampling conditions:

Sampling in a rectangular sampling grid. Sampling rates $\Delta x = 1/\sigma_1 N_1 \Delta f_x$; $\Delta y = 1/\sigma_2 N_2 \Delta f_y$

Non-zero sampling grid shift parameters (u, v) and (p, q)

$$\sigma_1 \sigma_2 \alpha_{r,s}^{u,v/p,q} = \sum_{k=0}^{N_1-1} \sum_{l=0}^{N_2-1} a_{k,l} \exp \left\{ i2\pi \left[\frac{(k+u)(r+v)}{\sigma_1 N_1} + \frac{(l+p)(s+q)}{\sigma_2 N_2} \right] \right\}$$

Rotated and Scaled DFTs

Sampling conditions:

- Sampling in a rectangular sampling grid in a rotated coordinate system $\begin{bmatrix} x^\theta \\ y^\theta \end{bmatrix} = \begin{bmatrix} \cos \theta & \sin \theta \\ -\sin \theta & \cos \theta \end{bmatrix} \begin{bmatrix} x \\ y \end{bmatrix}$ with θ as a rotation angle
- Sampling rates $\Delta x = 1/\sigma N \Delta f_x$; $\Delta y = 1/\sigma N \Delta f_y$; Non-zero sampling grid shift parameters (u, v) and (p, q)

$$\sigma \alpha_{r,s}^\theta \propto \sum_{k=0}^{N-1} \sum_{l=0}^{N-1} a_{k,l} \exp \left[i2\pi \left(\frac{\tilde{r}\tilde{k} + \tilde{s}\tilde{l}}{\sigma N} \cos \theta - \frac{\tilde{s}\tilde{k} - \tilde{r}\tilde{l}}{\sigma N} \sin \theta \right) \right];$$

$$\begin{aligned} \tilde{k} &= k + u; \quad \tilde{r} = r + v; \\ \tilde{l} &= l + p; \quad \tilde{s} = s + q \end{aligned}$$

Discrete representation of Fresnel integral transform

Fresnel integral Transform

$$\alpha(f) = \int_{-\infty}^{\infty} a(x) \exp\left(i2\pi \frac{(x-f)^2}{\lambda Z}\right)$$

Scaled Shifted Discrete Fresnel Transform

Sampling conditions:

Cardinal sampling rate $\Delta x = 1/\sigma N \Delta f$ with scale σ

Non-zero sampling grid shift parameters $(u, v) : w = u/\mu - v\mu$

$$\alpha_r^{(\mu, w)} = \frac{1}{\sqrt{N}} \sum_{k=0}^{N-1} a_k \exp\left[-i\pi \frac{(k\mu - r/\mu + w)^2}{\sigma N}\right]$$

Convolutional Discrete Fresnel Transform (ConvDFrT)

Sampling conditions: sampling rates: $\Delta x = \Delta f$

$$\begin{aligned} \alpha_r &= \frac{1}{N} \sum_{s=0}^{N-1} \left\{ \left[\sum_{k=0}^{N-1} a_k \exp\left(i2\pi \frac{ks}{N}\right) \right] \exp\left(-i\pi \frac{\mu^2 s^2}{N}\right) \right\} \exp\left(-i2\pi \frac{rs}{N}\right) = \\ &= \frac{1}{N} \sum_{s=0}^{N-1} \left[\sum_{k=0}^{N-1} a_k \exp\left(i2\pi \frac{k-r}{N} s\right) \right] \exp\left(-i\pi \frac{\mu^2 s^2}{N}\right) = \frac{1}{N} \sum_{k=0}^{N-1} a_k \left[\sum_{s=0}^{N-1} \exp\left(-i\pi \frac{\mu^2 s^2}{N}\right) \exp\left(i2\pi \frac{k-r}{N} s\right) \right] = \\ &= \sum_{k=0}^{N-1} a_k \text{frincd}(N; \mu^2; r-k) \end{aligned}$$

Point spread function of discrete Fourier analysis

$$\alpha_r = \int_{-\infty}^{\infty} \alpha(f) h_{DFA}(f, r) df$$

Spectrum
samples
computed
using ScDFT

Signal
continuous
spectrum

PSF of
discrete
spectral
analysis

$$h_{DFA}(f, r) = N \operatorname{sincd} \left[N; \left(\frac{r}{\sigma} - f N \Delta x \right) \right] \Phi_s(f)$$

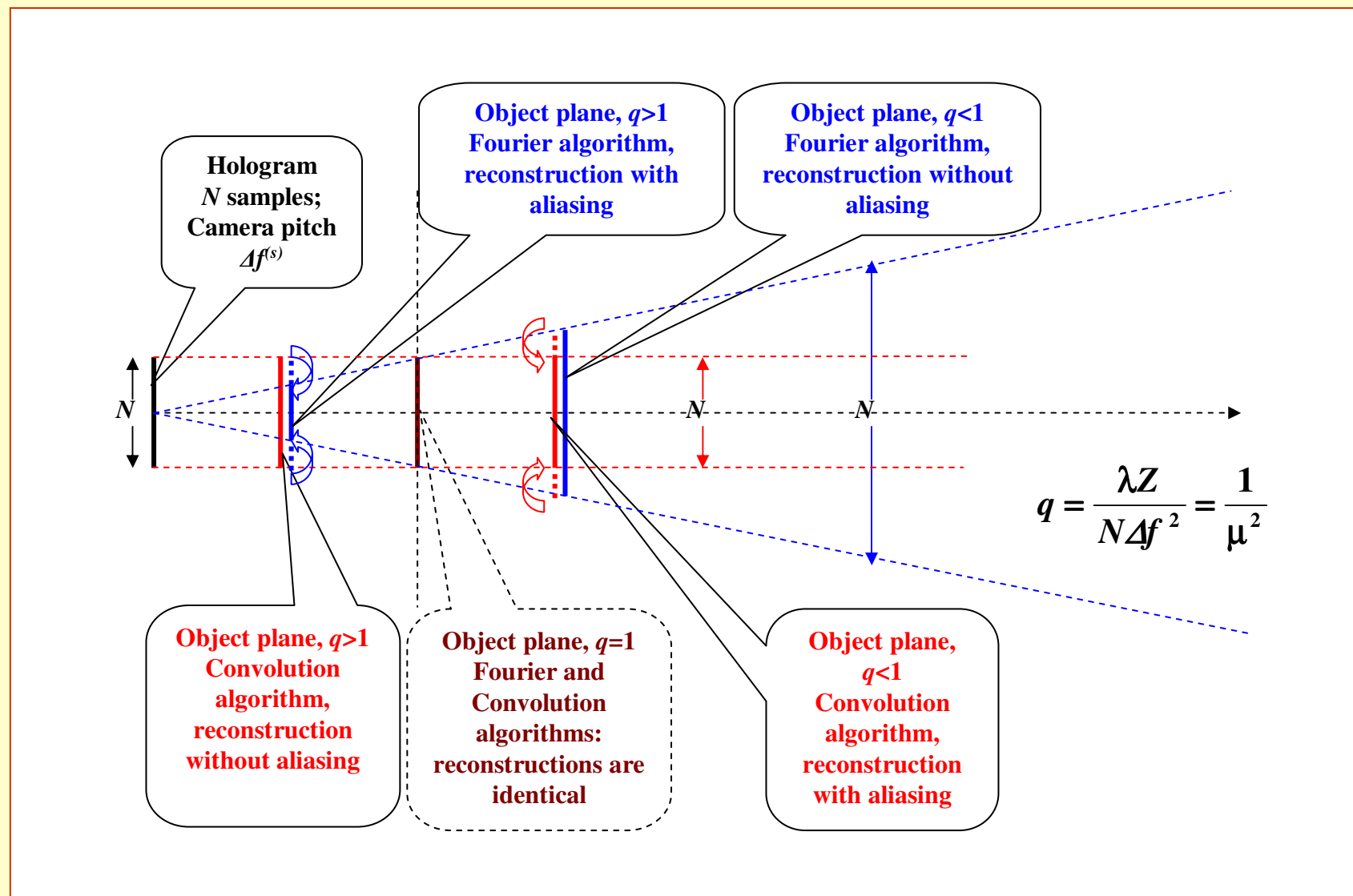
$$\operatorname{sincd}(N; x) = \frac{\sin x}{N \sin(x/N)}$$

N is the number of signal samples

σ – sampling scale parameter

Δx – sampling interval

Zones of applicability of Fourier and convolutional algorithms of reconstruction holograms recorded in near diffraction zone



Hologram reconstruction: Fourier algorithm vs Convolution algorithm

Hologram courtesy
Dr. J. Campos, UAB,
Barcelona, Spain

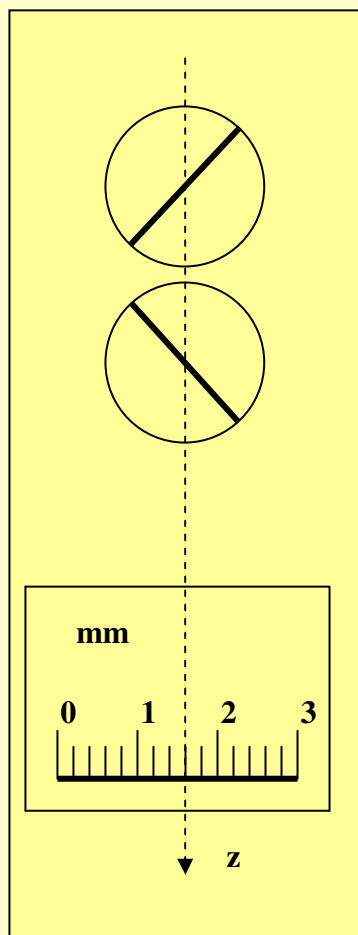


Image is
destroyed
due to
aliasing

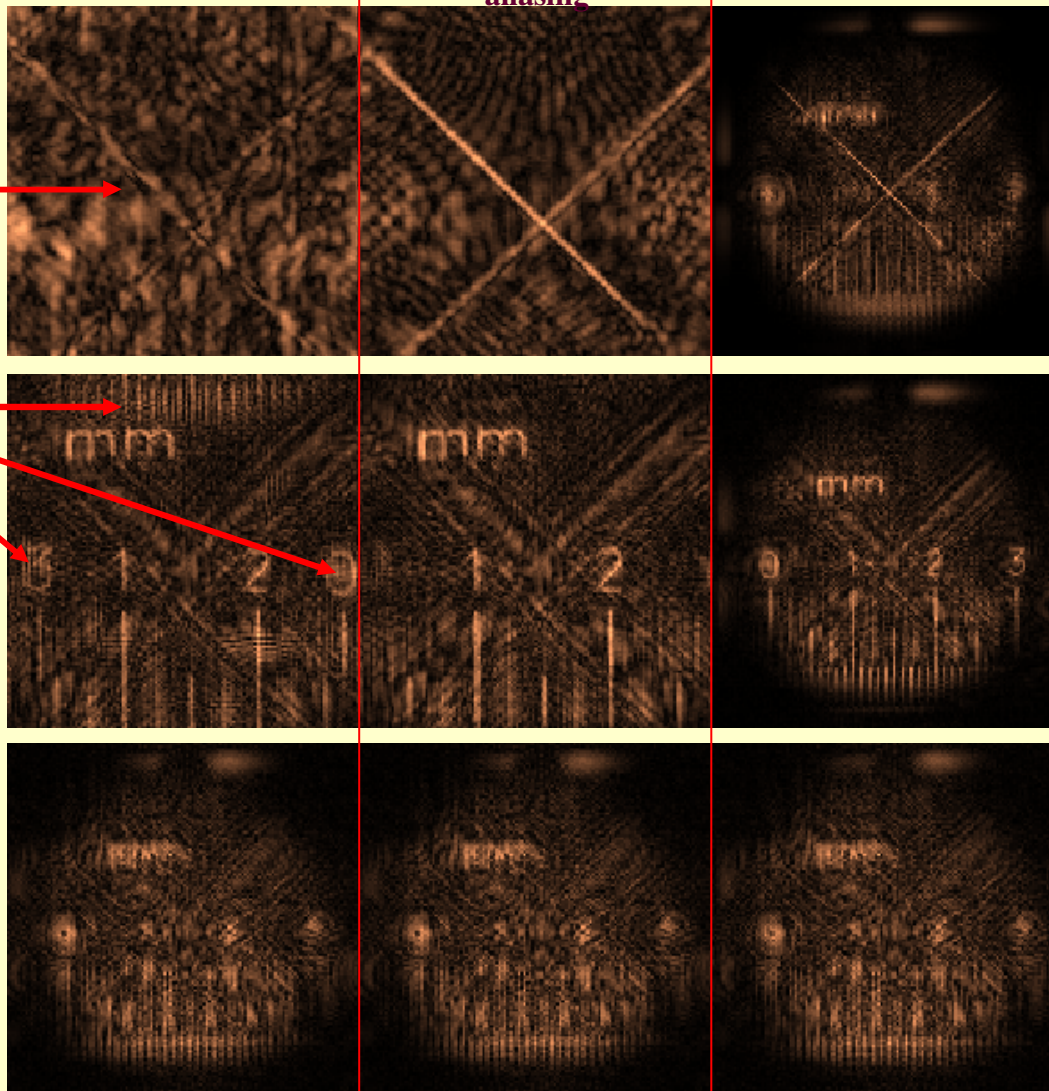
Aliasing
artifacts

All
restorations
are identical

Fourier
reconstruction

Fourier
reconstruction of
the central part of
the hologram free of
aliasing

Convolution
reconstruction

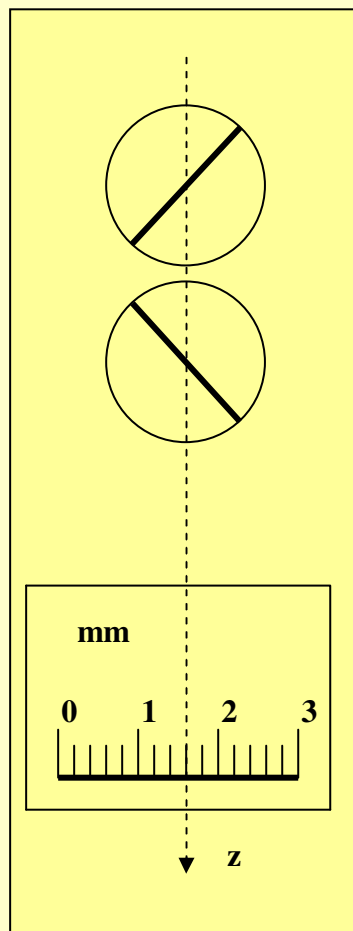


$Z=33\text{mm};$
 $\mu^2=0.2439$

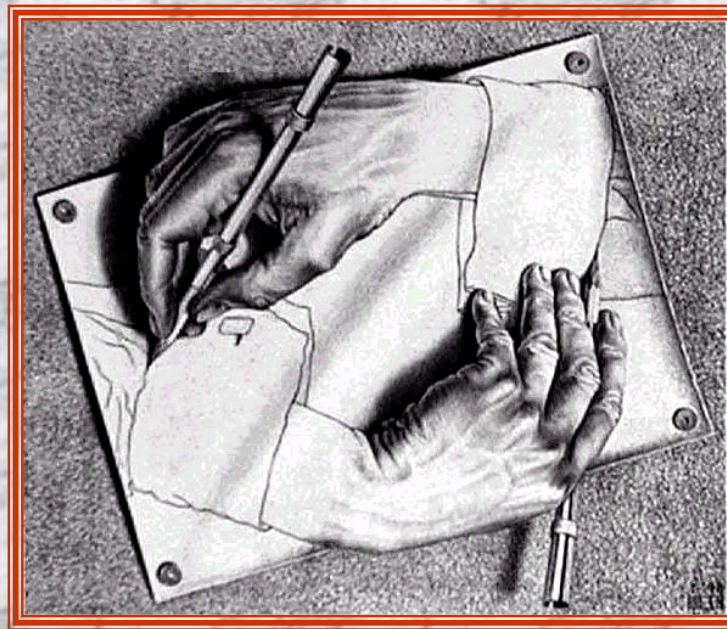
$Z=83\text{mm};$
 $\mu^2=0.6618$

$Z=136\text{mm};$
 $\mu^2=1$

Discretization aliasing artifacts in reconstruction of a hologram on different distances using Fourier reconstruction algorithm (left), the Fourier reconstruction algorithm with appropriate hologram masking to avoid aliasing (middle) and the Convolution reconstruction algorithm



BUILDING CONTINUOUS IMAGE MODELS



When working with sampled images in computers, one frequently needs to return back to their continuous originals. Typical applications that require restoration of continuous image models are image reconstruction from projections, multi-modality data fusion, target location and tracking with sub-pixel accuracy, image restoration from sparse samples and image differentiation and integration, to name a few.

**Discrete sinc-interpolation:
a gold standard
for image resampling**

Image resampling assumes reconstruction of the continuous approximation of the original non-sampled image by means of interpolation of available image samples to obtain samples in-between the given ones. In some applications, for instance, in computer graphics and print art, simple interpolation methods, such as nearest neighbor or linear (bilinear) interpolations, can provide satisfactory results. However, all these methods add interpolation error to reconstructed continuous image models, thus introducing signal distortions additional to those caused by the primary image sampling.

A discrete signal interpolation method that is capable to secure continuous image restoration without adding any additional interpolation errors is the discrete sinc-interpolation

Discrete sinc-interpolation is a discrete analog of the continuous sinc-interpolation, which, theoretically, secures error free reconstruction of band-limited signals from their samples and least mean square error reconstruction of arbitrary continuous signals, provided infinitely large number of signal samples is available.

Discrete sinc-interpolation does the same for discrete signals.

For the purposes of the design of the perfect resampling filter, one can regard signal co-ordinate shift as a general resampling operation.

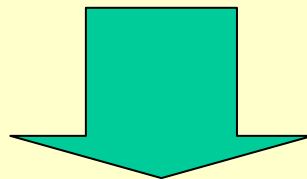
Signal resampling is a linear signal transformation. As any linear transformation, it can be fully characterized by its point spread function (PSF) or, correspondingly, by its overall frequency response.

The optimal shifting re-sampling filter is the filter that generates a shifted copy of the input signal with preservation of the analog signal spectrum in its base band defined by the signal sampling rate and by the number of available signal samples.

According to this definition, overall continuous frequency response $H^{(intp)}(p)$ of the optimal $\delta\tilde{x}$ - shifting filter for the coordinate shift $\delta\tilde{x}$ is, by virtue of the Fourier transform shift theorem,

$$H^{(intp)}(p) = \exp(i2\pi p \delta\tilde{x})$$

According to the discrete representation of the convolution integral, discrete frequency response coefficients $\{\eta_{r,opt}^{(intp)}(\delta\tilde{x})\}$ (DFT of its discrete PSF) of the optimal -shift re-sampling filter must be taken as samples, in sampling points $\{r/N\Delta x\}; r = 0, 1, \dots, N-1$, of its continuous frequency response, which, for the ideal signal sampling and reconstruction devices, coincides, within the signal base band, with the filter overall frequency response $H^{(intp)}(p) = \exp(i2\pi p \delta\tilde{x})$



Therefore for odd N

$$\eta_{r,opt}^{(intp)}(\tilde{\Delta x}) = \frac{1}{\sqrt{N}} \exp\left(i 2\pi \frac{r \tilde{\Delta x}}{N \Delta x}\right), \quad r = 0, 1, \dots, (N-1)/2$$
$$\eta_{r,opt}^{(intp)}(\tilde{\Delta x}) = \eta_{N-r,opt}^{*(intp)}(\tilde{\Delta x}), \quad r = (N+1)/2, \dots, N-1$$

and for even N :

$$\eta_{r,opt}^{(intp)}(\tilde{\Delta x}) = \begin{cases} \exp\left(i 2\pi \frac{r \tilde{\Delta x}}{N \Delta x}\right), & r = 0, 1, \dots, N/2 - 1 \\ A \cos\left(\pi \frac{\tilde{\Delta x}}{\Delta x}\right), & r = N/2 \end{cases}$$
$$\eta_{r,opt}^{(intp)}(\tilde{\Delta x}) = \left(\eta_{N-r,opt}^{(intp)}(\tilde{\Delta x})\right)^*, \quad r = N/2 + 1, \dots, N-1$$

The following three options for A are:

Case_0: $A=0$, Case_1: $A=1$, Case_2: $A=2$, .

Therefore, for odd N , point spread function of the optimal $\delta\tilde{x}$ -resampling (fractional shift) filter is

$$h_n^{(intp)}(\delta\tilde{x}) = \text{sincd}\{N, \pi[n - (N - 1)/2 - \delta\tilde{x}/\Delta x]\}.$$

For even N , Case_0 and Case_2, optimal resampling point spread functions are

$$h_n^{(intp0)}(\delta\tilde{x}) = \overline{\text{sincd}}\{N; N - 1; \pi[n - (N - 1)/2 - \delta\tilde{x}/\Delta x]\}$$

and

$$h_n^{(intp2)}(\delta\tilde{x}) = \overline{\text{sincd}}\{N; N + 1; \pi[n - (N - 1)/2 - \delta\tilde{x}/\Delta x]\},$$

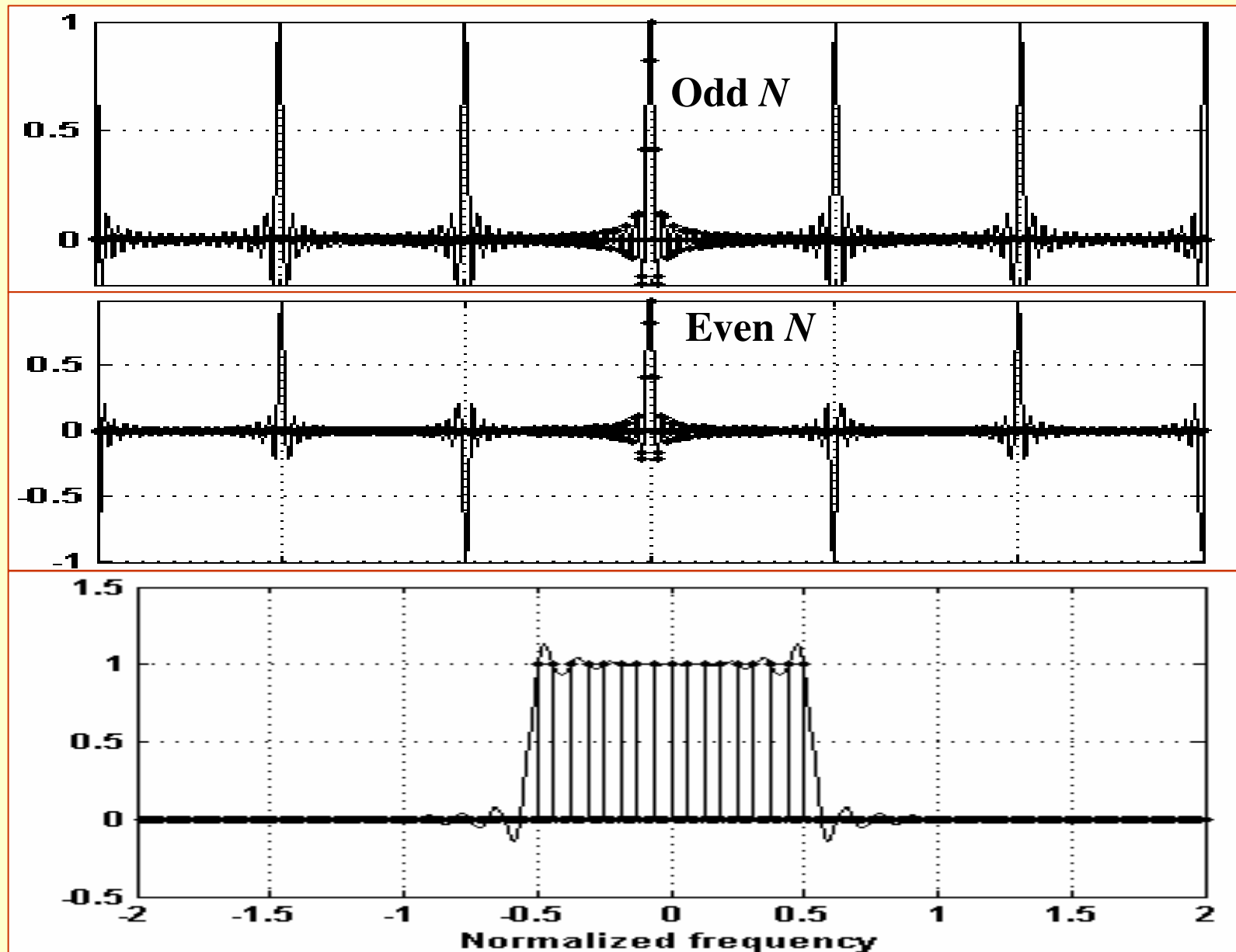
correspondingly, where a modified sincd-function $\overline{\text{sincd}}$ is defined as

$$\overline{\text{sincd}}(N; M; x) = \frac{\sin(Mx/N)}{N \sin(x/N)}$$

Case_1 is just a combination of Case_0 and Case_2:

$$h_n^{(intp2)}(\delta\tilde{x}) = [h_n^{(intp0)}(\delta\tilde{x}) + h_n^{(intp2)}(\delta\tilde{x})]/2 = \overline{\text{sincd}}(\pm 1; N; x) = [\overline{\text{sincd}}(N - 1; N; x) + \overline{\text{sincd}}(N + 1; N; x)]/2.$$

Point spread functions and frequency response of the discrete sinc-interpolators



The above results can be formulated as a theorem:

For analog signals defined by their N samples, discrete sinc-interpolation is, for odd N , the only discrete convolution based signal re-sampling method that does not distort signal spectrum samples in its base band specified by the signal sampling rate ; for even N , discrete sinc-interpolation distorts only the highest $N/2$ -th frequency spectral component.

Implementation issues:

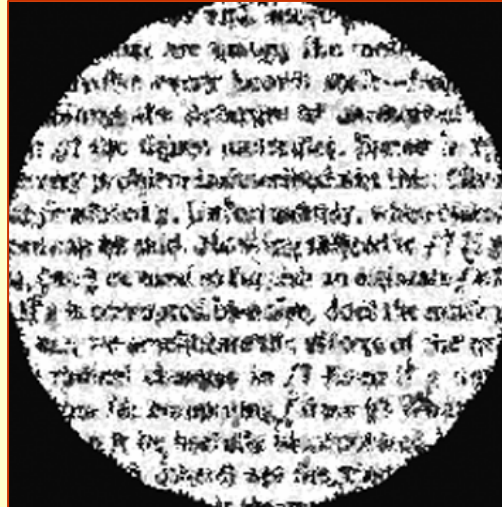
The described $\tilde{\delta x}$ -resampling filter that implements discrete sinc-interpolation is designed in DFT domain. Therefore it can be straightforwardly implemented using Fast Fourier Transform with the computational complexity of $O(\log N)$ operations per output signal sample, which makes it competitive with other less accurate interpolation methods.

From the application point of view, the only drawback of such an implementation is that it tends to produce signal oscillations due to the boundary effects caused by the circular periodicity of convolution implemented in DFT domain. These oscillation artifacts can be virtually completely eliminated, if discrete sinc-interpolation convolution is implemented in DCT domain

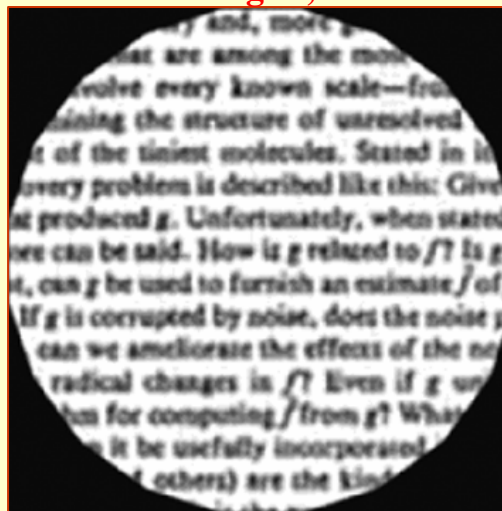
Interpolation accuracy comparison: 16x18° - image rotation

Image recovery and, more generally, signal processing problems that are among the most fundamental involve every known scale—from the determining the structure of unresolved stars to the determination of the tiniest molecules. Stated in its simplest form, the recovery problem is described like this: Given a noisy observation g , can we produce an estimate \hat{f} of f ? Unfortunately, when stated like this, not much more can be said. How is g related to f ? Is g a noisy version of f ? If so, can g be used to furnish an estimate \hat{f} of f ? If g is corrupted by noise, does the noise prevent us from recovering f ? If so, can we ameliorate the effects of the noise? Can we detect radical changes in f ? Even if g is a noisy version of f , is there a unique algorithm for computing \hat{f} from g ? What about the stability of \hat{f} ? Can it be usefully incorporated in our existing knowledge of f ? These (and others) are the kinds of questions that arise in the study of image recovery itself. It is the purpose of this book to provide a comprehensive survey of the state of the art in this field.

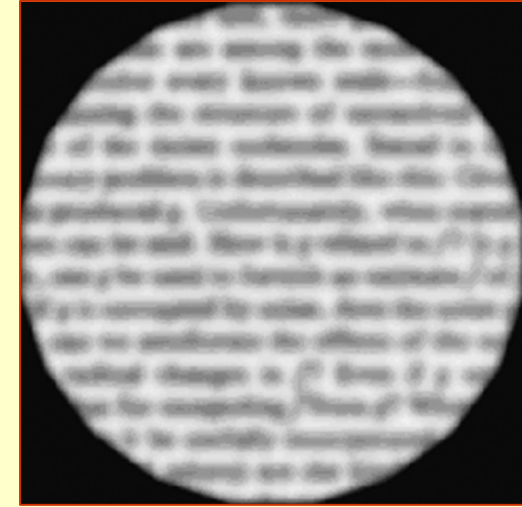
Test image



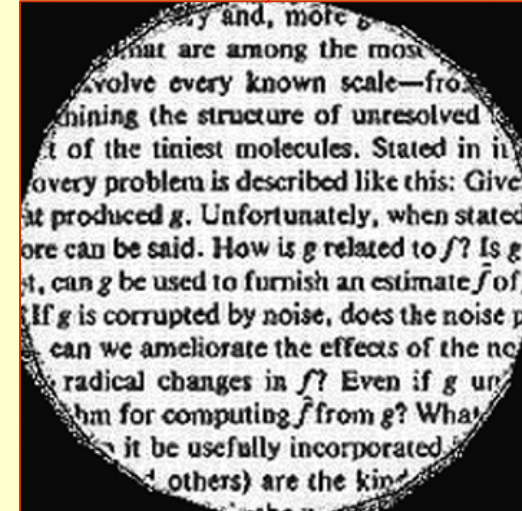
NearNeighb, T=7.27



Bicubic, T=17.7



Bilinear, T=11.1

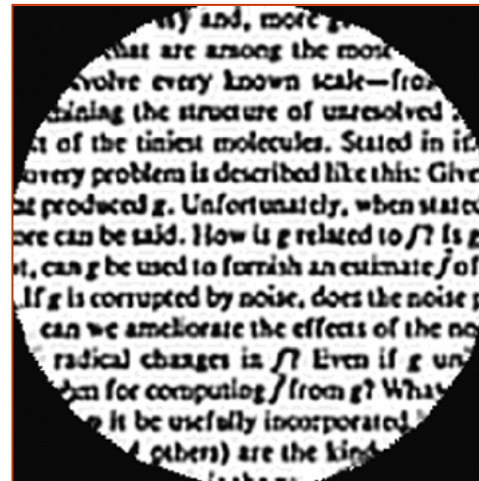


Discrete sinc, T=14.2

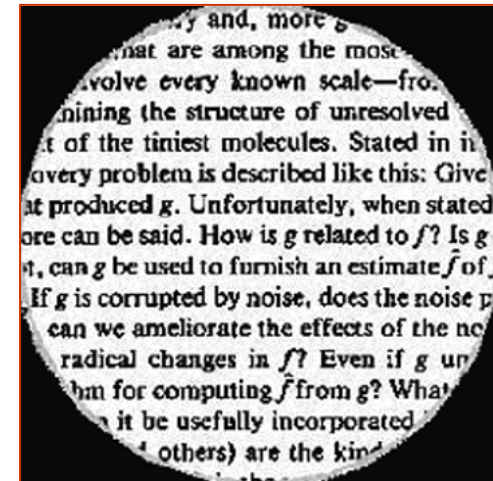
Discrete sinc-interpolation vs spline (Mems531) interpolation: Image 1000x18° rotation

Image recovery and, more generally, signal processing problems that are among the most fundamental in science involve every known scale—from the determining the structure of unresolved stars to the determination of the tiniest molecules. Stated in its most general form, the recovery problem is described like this: Given a set of data g produced by a process f , can we recover f from g ? Unfortunately, when stated in this form, not much can be said. How is g related to f ? Is g a noisy version of f ? If so, can g be used to furnish an estimate \hat{f} of f ? If g is corrupted by noise, does the noise prevent us from recovering f ? If so, can we ameliorate the effects of the noise? Does f have any special properties? If so, can we use these to recover f more radically than in g ? Even if g is unique, can we find a simple algorithm for computing \hat{f} from g ? What about the stability of \hat{f} ? Can it be usefully incorporated in our existing knowledge of f ? These (and others) are the kinds of questions that arise in the study of image recovery. It is the purpose of this book to provide a comprehensive survey of the state of the art in this field.

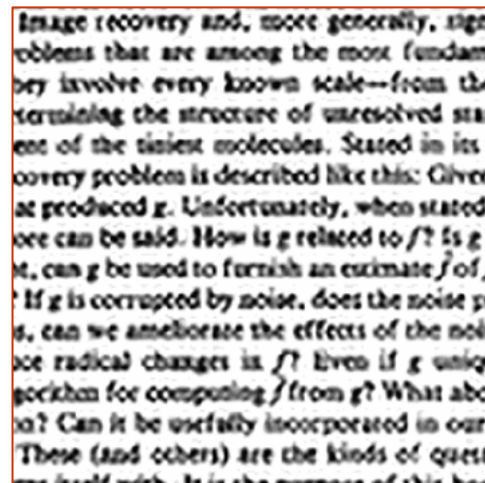
Test image



Spline Mems531-interpolation

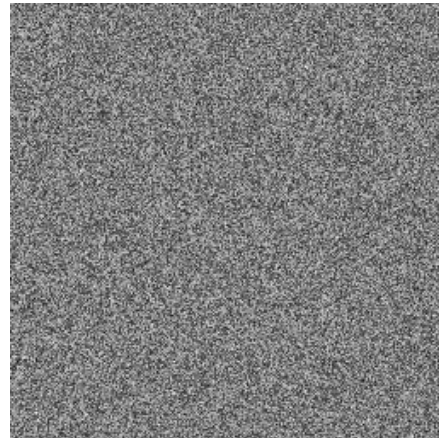


Discrete sinc-interpolation

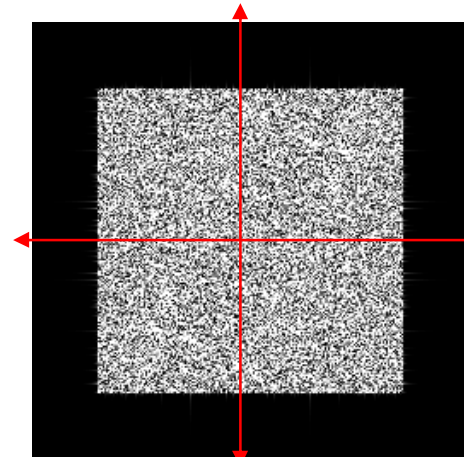


Test image low-pass filtered tp 0.4 of its bandwidth

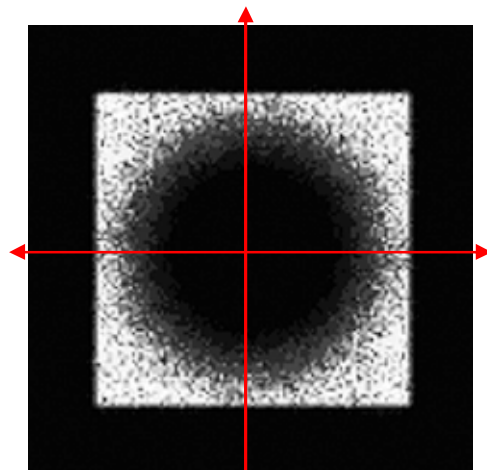
Discrete sinc interpolation vs spline (Mems531) interpolation: Rotation error DFT spectra comparison (image 10x36° rotation)



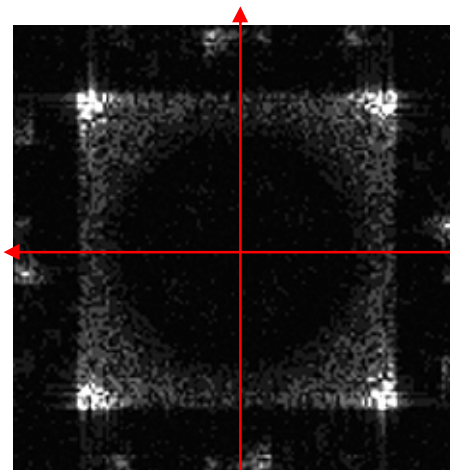
Pseudo-random test image



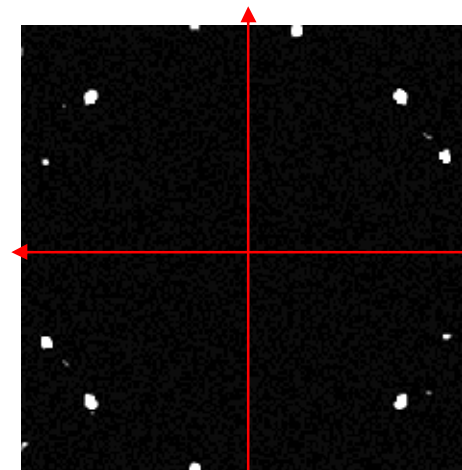
Test image DFT spectrum



Bicubic interpolation



Mems531 interpolation



Discrete sinc interpolation

DFT spectra of rotated image error (dark- small errors; bright – large errors)

Image numerical differentiation and integration

Signal numerical differentiation and integration are operations that are defined for continuous signals and require measuring infinitesimal increments or decrements of signals and their arguments. Therefore, numerical computing signal derivatives and integrals assumes one or another method of building continuous models of signals specified by their samples through explicit or implicit interpolation between available signal samples.

Differentiation and integration are shift invariant linear operations. Hence methods of computing signal derivatives and integrals from their samples can be conveniently designed, implemented and compared in the Fourier transform domain.

Signal differentiation and integration can be regarded as signal linear filtering with filter frequency responses, correspondingly

$$H_{diff}(f) = -i2\pi f \quad \text{and} \quad H_{int}(f) = i/2\pi f$$

Then coefficients $\{\eta_{r,opt}^{(diff)}\}$ and $\{\eta_{r,opt}^{(int)}\}$ of discrete frequency responses of numerical differentiation and integration digital filters defined as samples of corresponding continuous frequency responses are:

$$\eta_{r,opt}^{(diff)} = \begin{cases} -i2\pi r / N, & r = 0, 1, \dots, N/2 - 1 \\ -\pi/2, & r = N/2 \\ i2\pi(N-r)/N, & r = N/2 + 1, \dots, N-1 \end{cases}; \quad \eta_{r,opt}^{(int)} = \begin{cases} 0, & r = 0 \\ iN/2\pi r, & r = 1, \dots, N/2 - 1 \\ -\pi/2, & r = N/2 \\ iN/2\pi(N-r), & r = N/2 + 1, \dots, N-1 \end{cases}$$

for even N and

$$\eta_r^{diff} = \begin{cases} -i2\pi r / N, & r = 0, 1, \dots, (N-1)/2 - 1 \\ i2\pi(N-r)/N, & r = (N+1)/2, \dots, N-1 \end{cases}; \quad \eta_r^{(int)} = \begin{cases} iN/2\pi r, & r = 0, 1, \dots, (N-1)/2 - 1 \\ iN/2\pi(N-r), & r = (N+1)/2, \dots, N-1 \end{cases}$$

for odd N .

Accurate numerical differentiation and integration: implementation issues

One can show that numerical differentiation and integration according above equations imply the discrete sinc-interpolation of signals. Being designed in DFT domain, the differentiation and integration filters can be efficiently implemented in DFT domain using Fast Fourier Transforms with the computational complexity of the algorithms of $O(\log N)$ operations per signal sample.

Likewise all DFT based discrete sinc interpolation algorithms, DFT-based differentiation and integration algorithms, being the most accurate in term of representation of the corresponding continuous filters within the signal base band, suffer from boundary effects. Obviously, DFT based differentiation is especially vulnerable in this respect.

This drawback can be efficiently overcome by means of even extension of signals to double length through mirror reflection at their boundaries before applying above described DFT based algorithms. For such extended signals, DFT based differentiation and integration are reduced to using fast DCT and IDcST algorithms instead of FFT:

$$\{\dot{a}_k\} = \text{IDcST}(\{\eta_{r,opt}^{(diff)}\} \bullet \text{DCT}(\{a_k\})) = \frac{2\pi}{N\sqrt{2N}} \sum_{r=1}^{N-1} r \alpha_r^{(DCT)} \sin\left(\pi \frac{k+1/2}{N} r\right);$$

$$\{\bar{a}_k\} = \text{IDcST}(\{\eta_{r,opt}^{(diff)}\} \bullet \text{DCT}(\{a_k\})) = \frac{\sqrt{N}}{2\pi\sqrt{2}} \sum_{r=1}^{N-1} \frac{\alpha_r^{(DCT)}}{r} \sin\left(\pi \frac{k+1/2}{N} r\right)$$

with the same computational complexity of $O(\log N)$ operations per signal sample

Conventional numerical differentiation and integration methods

In numerical mathematics, alternative methods of numerical computing signal derivatives and integrals are commonly used that are implemented through signal discrete convolution in the signal domain:

$$\dot{a}_k = \sum_{n=0}^{N_h-1} h_n^{diff} a_{k-n} ; \bar{a}_k = \sum_{n=0}^{N_h-1} h_n^{int} a_{k-n} .$$

Commonly, the simplest differentiating kernels of two and five samples are recommended

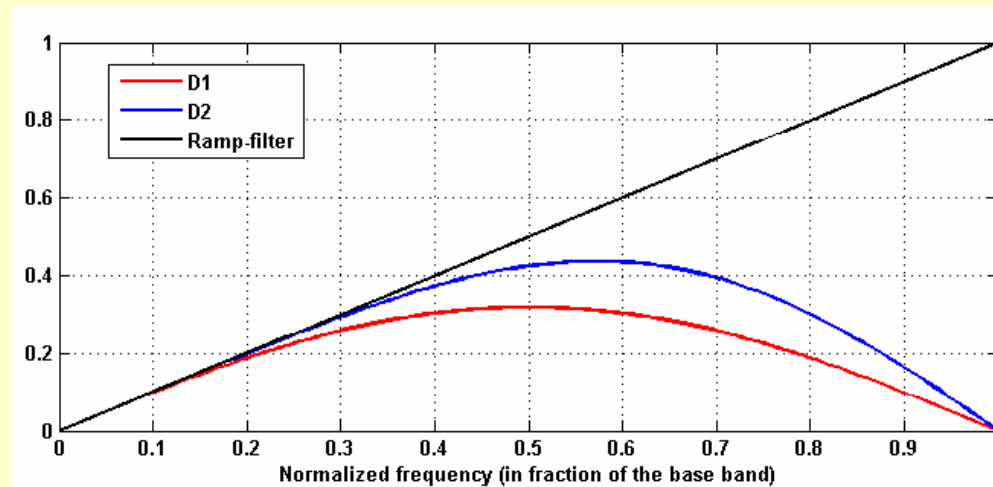
$$\text{D1: } h_n^{diff(1)} = [-0.5, 0, 0.5]; \quad \text{D2: } h_n^{diff(2)} = [-1/12, 8/12, 0, -8/12, 1/12].$$

Most known numerical integration methods are the *Newton-Cotes quadrature rules*. The three first rules are the trapezoidal, the Simpson and the 3/8 Simpson ones defined, for k as a running sample index, as, respectively:

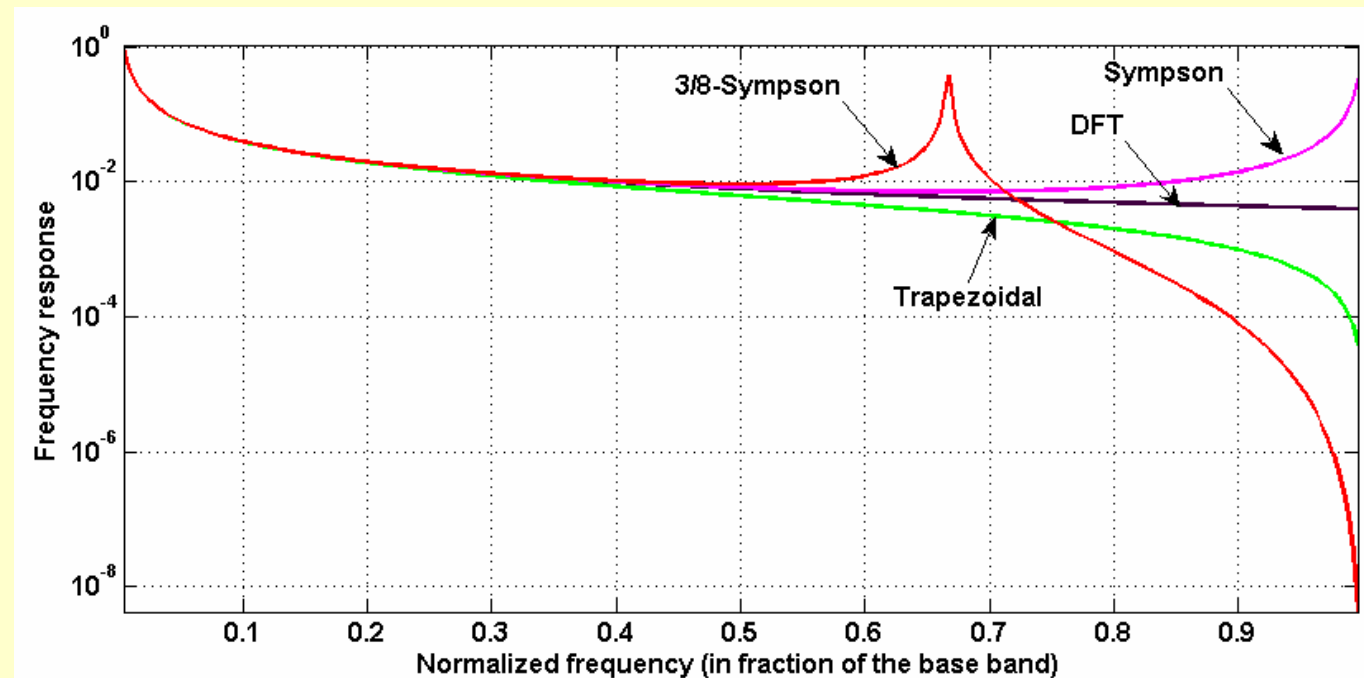
$$\bar{a}_1^{(T)} = 0, \quad \bar{a}_k^{(T)} = \bar{a}_{k-1}^{(T)} + \frac{1}{2}(a_{k-1} + a_k); \quad \bar{a}_1^{(S)} = 0, \quad \bar{a}_k^{(S)} = \bar{a}_{k-2}^{(S)} + \frac{1}{3}(a_{k-2} + 4a_{k-1} + a_k).$$

$$\bar{a}_0^{(3/8S)} = 0, \quad \bar{a}_k^{(3/8S)} = \bar{a}_{k-3}^{(3/8S)} + \frac{3}{8}(a_{k-3} + 3a_{k-2} + 3a_{k-1} + a_k).$$

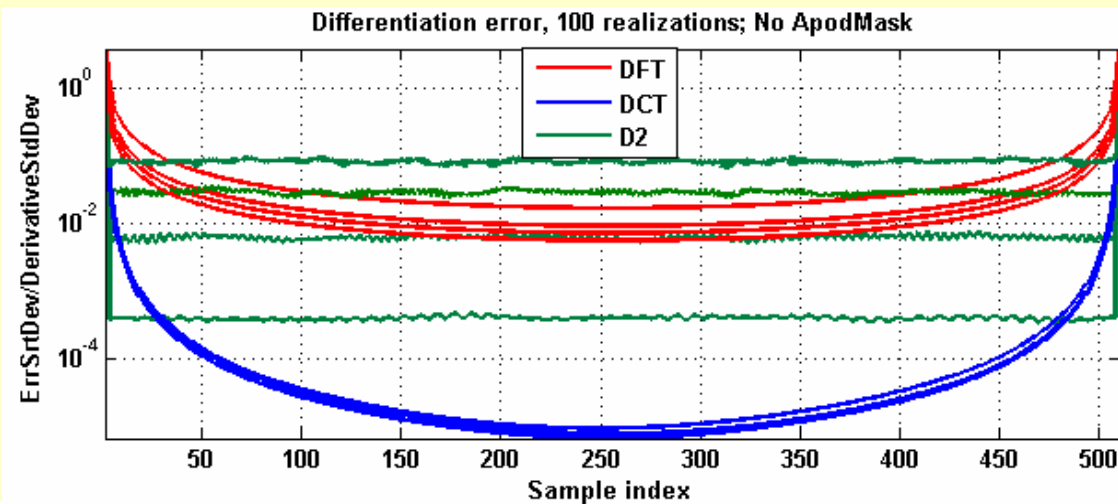
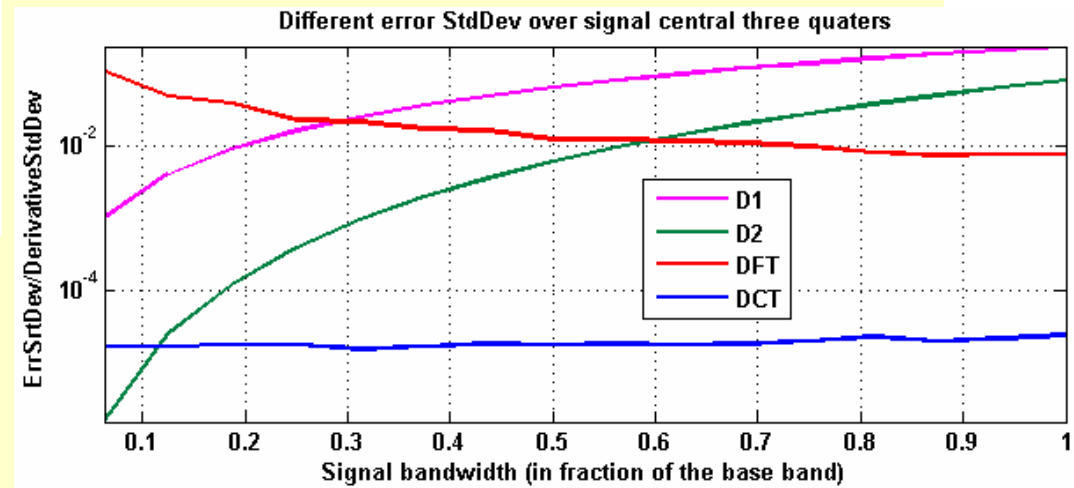
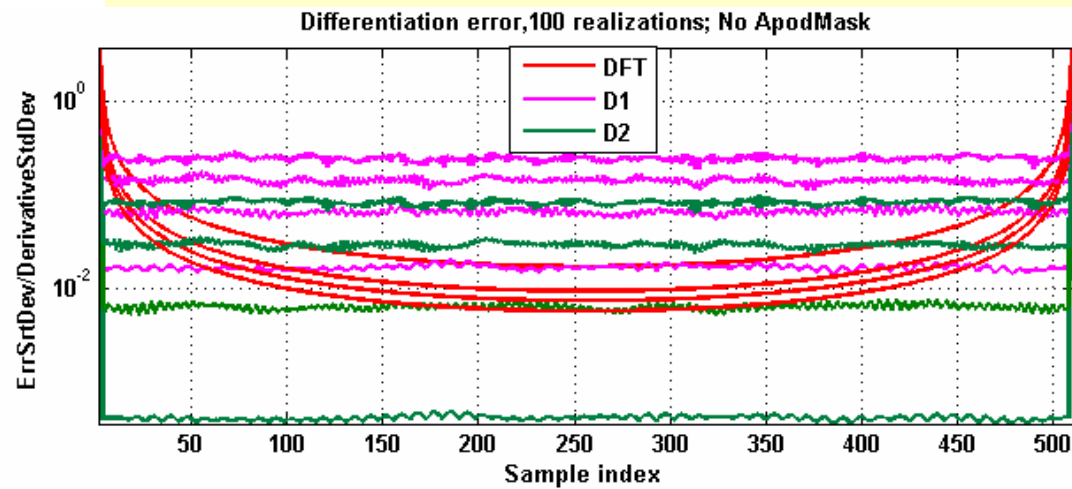
Frequency responses of numerical differentiation methods



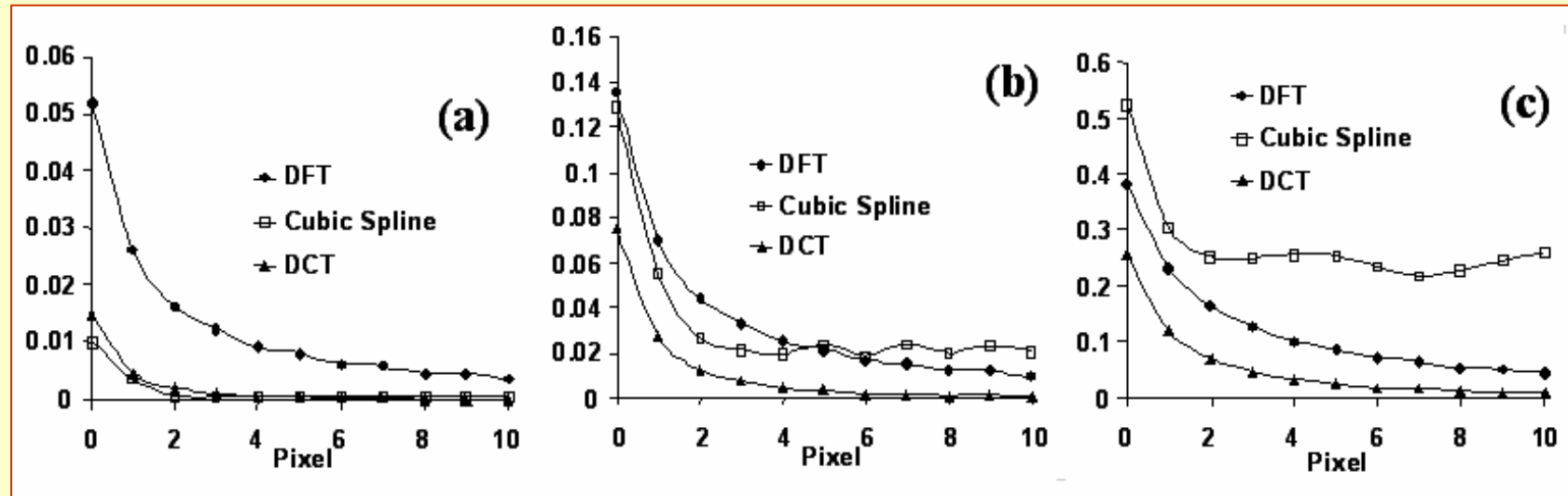
Frequency responses of numerical integration methods



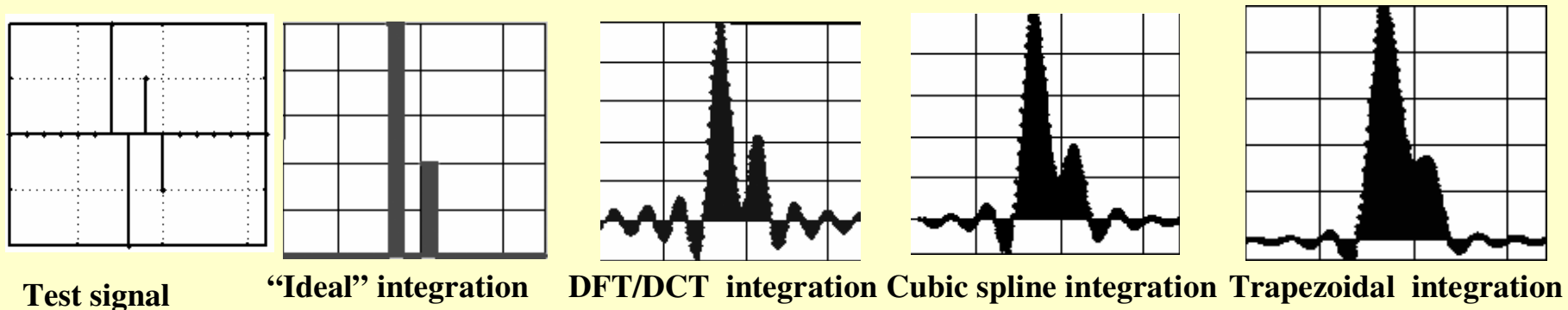
Differentiation error comparison



Numerical integration error comparison

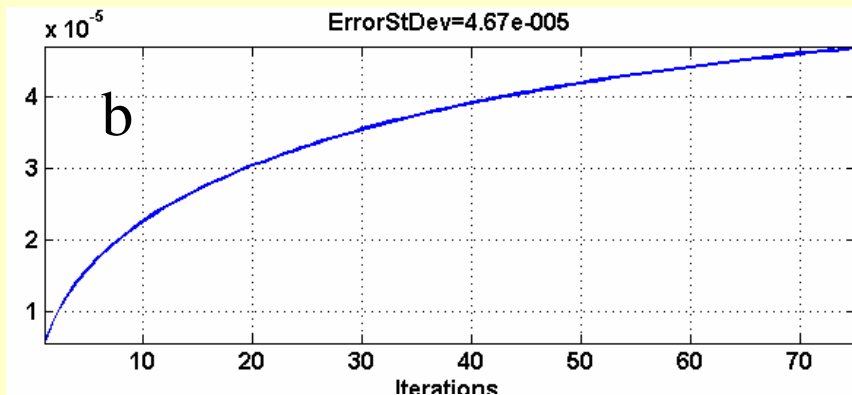
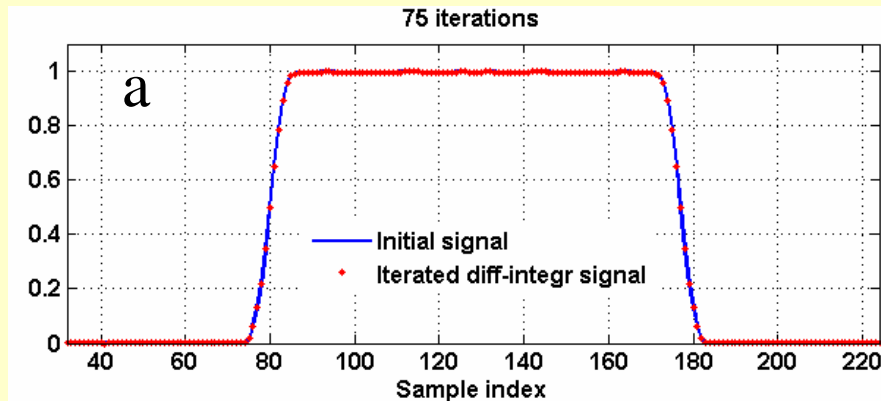


Resolving power of numerical integrators

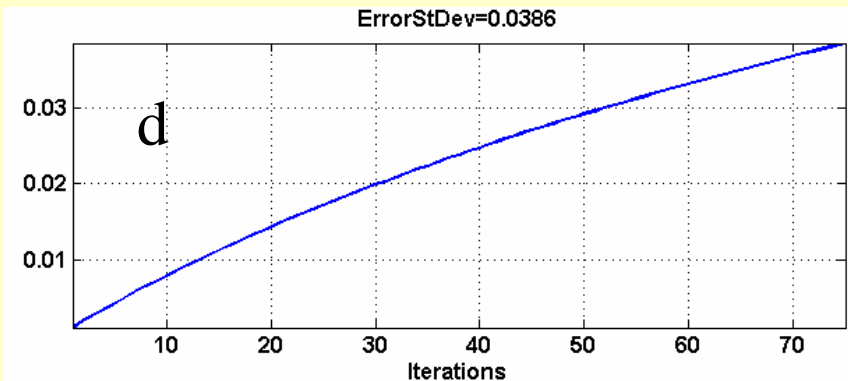
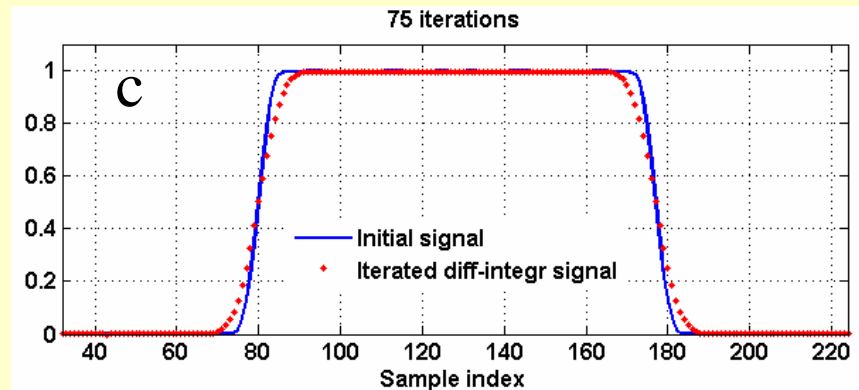


DCT based versus conventional differentiation-integration methods: signal restoration error

DCT-based differentiation and integration



D2 differentiation & trapezoidal integration



Comparison of standard deviations signal restoration error after iterative successive 75 differentiations and integrations applied to a test signal for DCT-based differentiation and integration methods and for D2 differentiator and trapezoidal rule integrator, respectively: a), c) – initial (blue curves) and restored (red dots) signals; b), d) – restoration error standard deviation vs the number of iterations

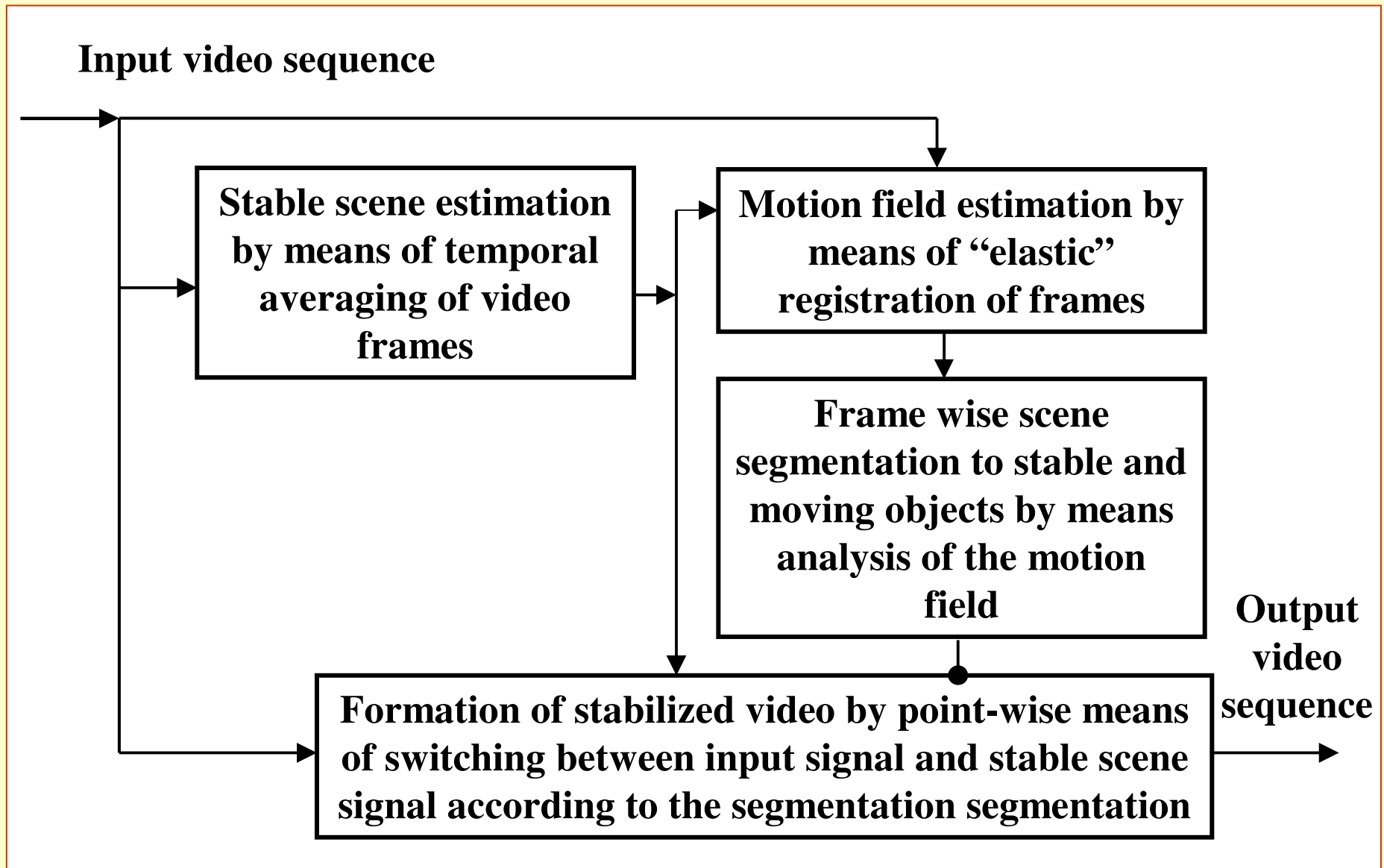
The background of the slide is a full-page image of marbled paper. It features a complex, organic pattern of swirling, interlocking shapes in various shades of beige, cream, and light brown, creating a textured, stone-like appearance.

COMPUTATIONAL IMAGING IN EXAMPLES

Case study: Real time stabilization and super-resolution of turbulent videos

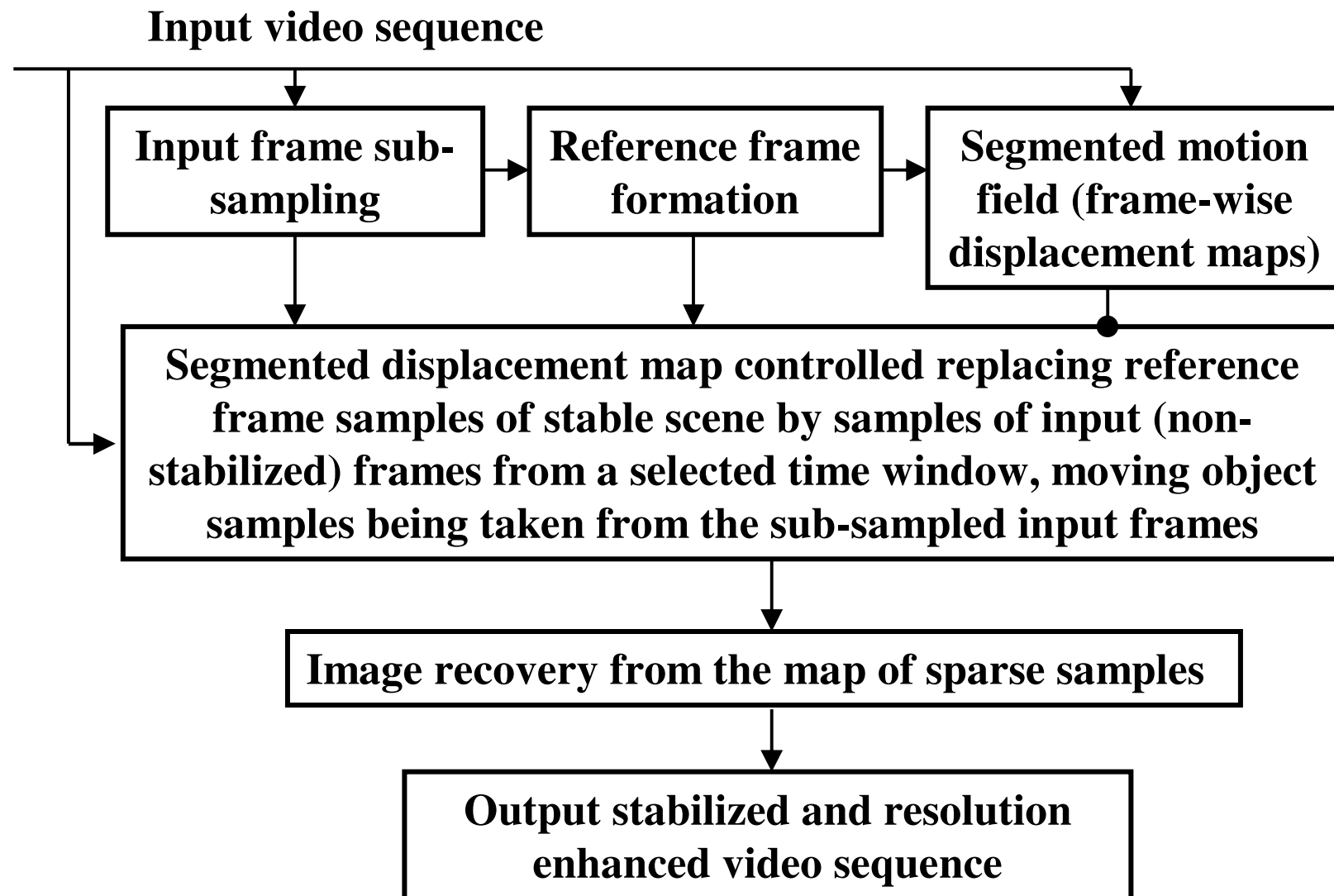


The video stabilization algorithm

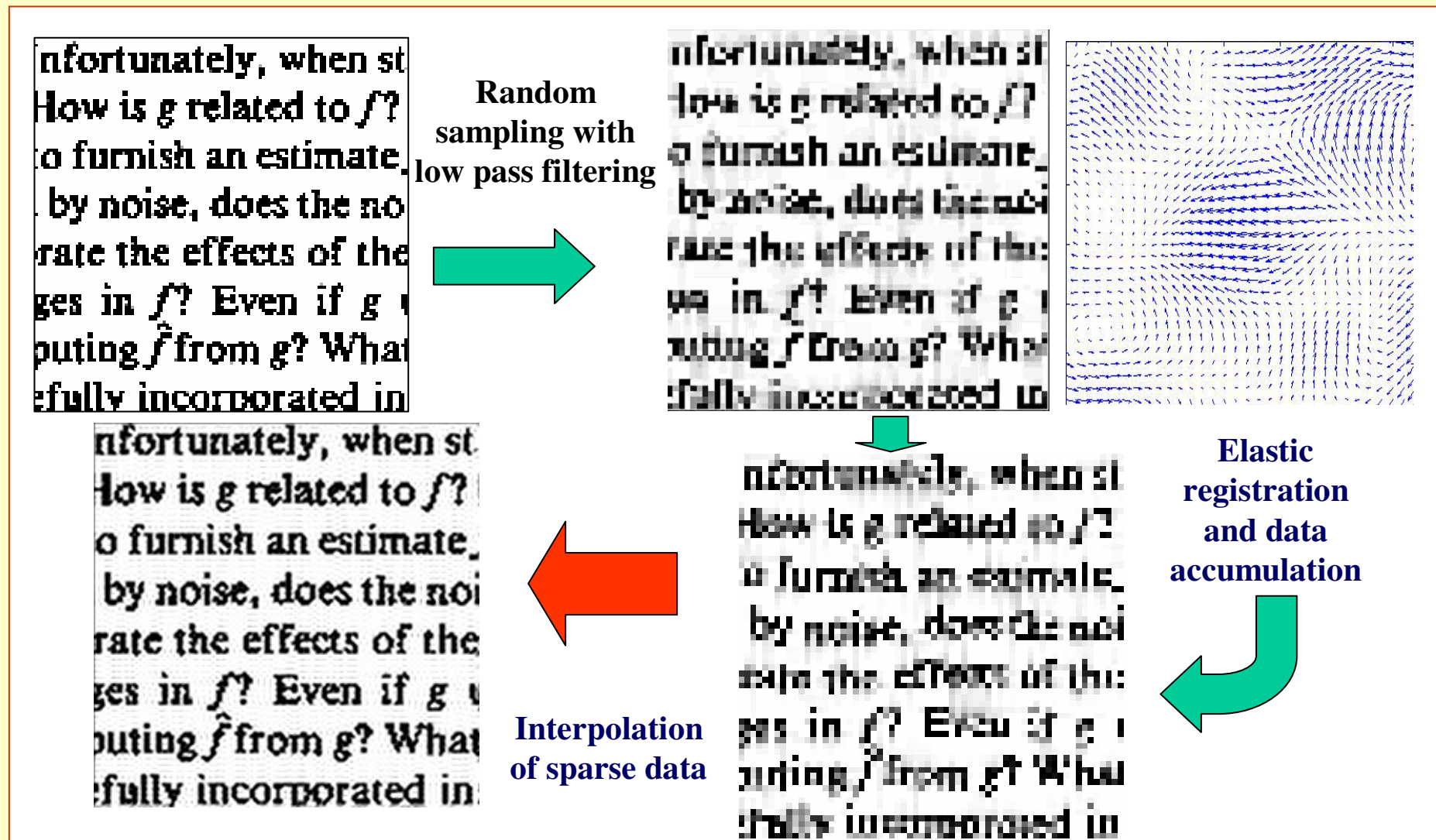




The super-resolution algorithm



Super-resolution in turbulent videos



Low resolution frames upper right); image fused by elastic image registration from 50 frames (bottom right); a result of iterative interpolation of the middle image after 50 iterations (bottom left).

Turbulent video stabilization and super- resolution

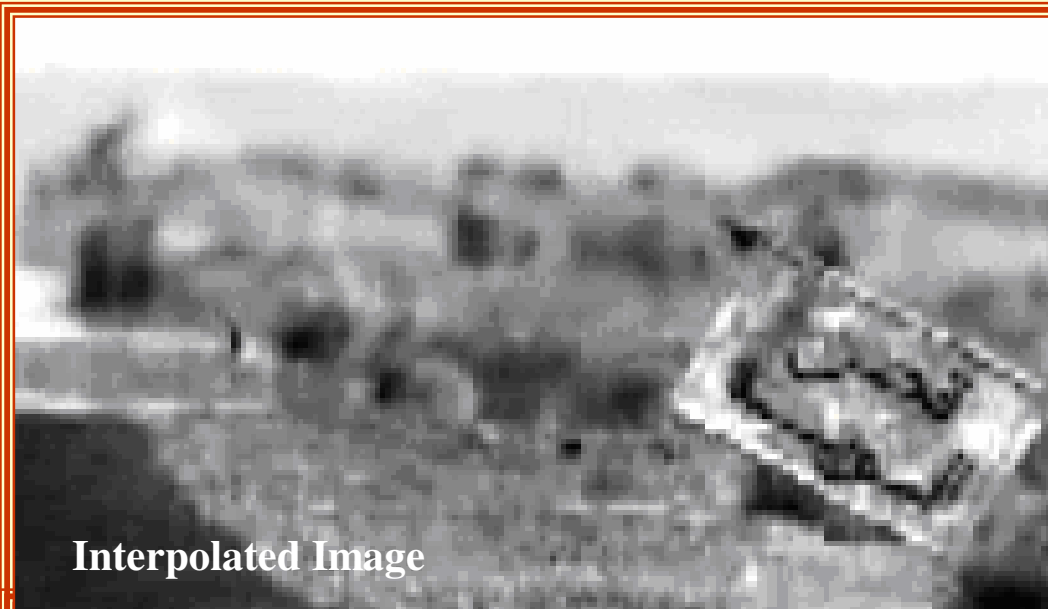
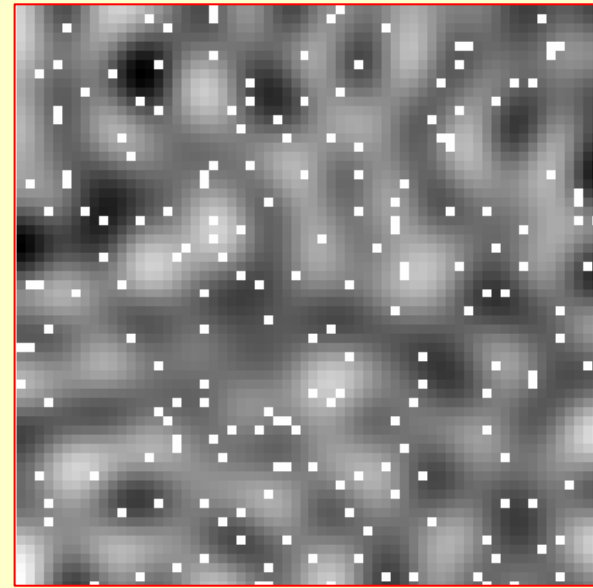
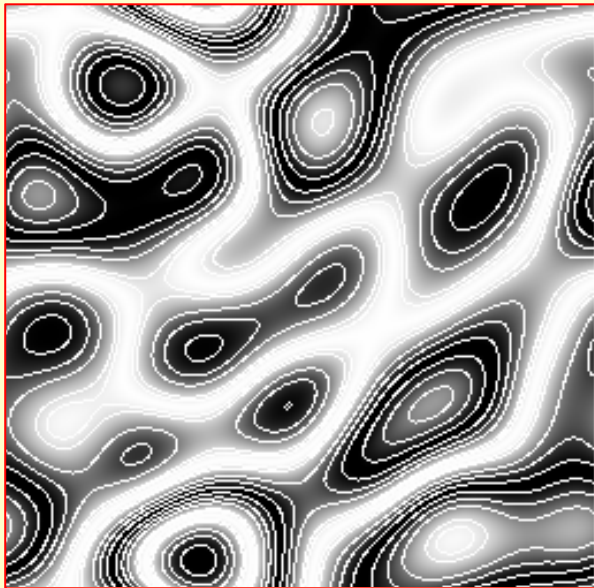


Image recovery from sparse data and the discrete sampling theorem

Shannon-Kotelnikov's sampling theorem tells how to optimally sample continuous signals and reconstruct them from the result of sampling with minimal MSError. This optimal sampling assumes a uniform sampling grid.

In many applications sampled data are collected in an irregular fashion or are partly lost or unavailable. In these cases it is required to convert irregularly sampled signals to regularly sampled ones, or to restore missing data.



We address this problem in a framework of the discrete sampling theorem for “band-limited” discrete signals that have a limited number of non-zero transform coefficients in the domain of a certain orthogonal transform.

Basic assumptions:

- Continuous signals are represented in computers by their samples.
- Let the number of signal samples on a regular sampling grid that are believed to fully represent the original continuous signal is N
- Let available be $K < N$ samples of this signal, taken at arbitrary positions of the signal regular sampling grid.
- The goal of the processing is generating, out of this “incomplete” set of samples, the complete set of N signal samples with the best possible accuracy.
- For definiteness, we will use restoration mean square error for evaluating signal approximation accuracy.

Discrete Sampling Theorem: preliminaries

Let \mathbf{A}_N be a vector of N samples $\{a_k\}_{k=0,\dots,N-1}$, which completely define a discrete signal, Φ_N be an $N \times N$ orthogonal transform matrix $\Phi_N = \{\varphi_r(k)\}_{r=0,1,\dots,N-1}$ and Γ_N be a vector of signal transform coefficients $\{\gamma_r\}_{r=0,\dots,N-1}$ such that

$$\mathbf{A}_N = \Phi_N \Gamma_N = \left\{ \sum_{r=0}^{N-1} \gamma_r \varphi_r(k) \right\}_{k=0,1,\dots,N-1}$$

Assume now that available are only $K < N$ samples $\{a_{\tilde{k}}\}_{\tilde{k} \in \tilde{\mathbf{K}}}$, where $\tilde{\mathbf{K}}$ is a K -size non-empty subset of indices $\{0,1,\dots,N-1\}$. These available K signal samples define a system of equations:

$$\left\{ a_k = \sum_{r=0}^{N-1} \gamma_r \varphi_r(k) \right\}_{k \in \tilde{\mathbf{K}}}$$

for signal transform coefficients $\{\gamma_r\}$ of certain K indices r .

Select now a subset \tilde{R} of K transform coefficients indices $\{\tilde{r} \in \tilde{R}\}$ and define a “KofN”-band-limited approximation to the signal as the

$$\hat{A}_N^{BL} = \left\{ \hat{a}_k = \sum_{\tilde{r} \in \tilde{R}} \gamma_{\tilde{r}} \phi_{\tilde{r}}(k) \right\}$$

Rewrite this equation in a more general form: $\hat{A}_N^{BL} = \left\{ \hat{a}_k = \sum_{r=0}^{N-1} \tilde{\gamma}_r \phi_r(k) \right\}$

and assume that all transform coefficients with indices $r \notin \tilde{R}$ are set to zero:

$$\tilde{\gamma}_r = \begin{cases} \gamma_r, & r \in \tilde{R} \\ 0, & r \notin \tilde{R} \end{cases}$$

Then the vector \tilde{A}_K of available signal samples $\{a_{\tilde{k}}\}_{\tilde{k} \in \tilde{K}}$ can be expressed in terms of the basis functions $\{\phi_r(k)\}$ of transform Φ_N as:

$$\tilde{A}_K = \text{KofN}_{\Phi} \cdot \tilde{I}_K = \left\{ \tilde{a}_{\tilde{k}} = \sum_{\tilde{r} \in \tilde{R}} \gamma_{\tilde{r}} \phi_{\tilde{r}}(\tilde{k}) \right\}$$

and the vector $\tilde{I}_K = \{\gamma_{\tilde{r}}\}$ of signal non-zero transform coefficients can be found as

$$\tilde{I}_K = \{\gamma_{\tilde{r}}\} = \text{KofN}_{\Phi}^{-1} \cdot \tilde{A}_K$$

In L2 norm, by virtue of the Parseval's theorem, the band-limited signal \hat{A}_N^{BL} approximates the complete signal A_N with mean squared error

$$MSE = \|A_N - \hat{A}_N\|^2 = \sum_{k=0}^{N-1} |a_k - \hat{a}_k|^2 = \sum_{r \notin \tilde{R}} |\gamma_r|^2$$

The Discrete Sampling Theorem

Statement 1. For any discrete signal of N samples defined by its $K \leq N$ sparse and not necessarily regularly arranged samples, its band-limited, in terms of a certain transform Φ_N , its approximation can be obtained with mean square error

$$MSE = \|A_N - \hat{A}_N\|^2 = \sum_{k=0}^{N-1} |a_k - \hat{a}_k|^2 = \sum_{r \notin R} |\gamma_r|^2$$

provided that positions of the samples secure the existence of the matrix \mathbf{KofN}_Φ^{-1} inverse to the sub-transform matrix \mathbf{KofN}_Φ that corresponds to the band-limitation. The approximation error can be minimized by using a transform with the best energy compaction property.

Statement 2. Any signal of N samples that is known to have only $K \leq N$ non-zero transform coefficients for certain transform Φ_N (Φ_N - “band-limited” signal) can be fully recovered from exactly K of its samples provided the positions of the sample secure the existence of the matrix \mathbf{KofN}_Φ^{-1} inverse to the transform sub-matrix \mathbf{KofN}_Φ that corresponds to the band-limitation.

Analysis of transforms: DFT

Low-pass DFT band- limited signals:

$$\tilde{r}_{LP} \in \tilde{R}_{LP} = \{[0,1,...,(K-1)/2,N-(K-1)/2,...,N-1]\}$$

\mathbf{KofN}_{DFT}^{LP} DFT -trimmed matrix $\mathbf{KofN}_{DFT}^{LP} = \left\{ \exp\left(i2\pi \frac{\tilde{k}\tilde{r}_{LP}}{N}\right) \right\}$ is a

Vandermonde matrix, and, as such, it can be inverted

Theorem 1.

Low-pass DFT band-limited signals of N samples with only K nonzero low frequency DFT coefficients can be precisely recovered from exactly K of their samples taken in arbitrary positions

High-pass DFT band-limited signals:

$$\tilde{r}_{HP} \in \tilde{R}_{HP} = \{[(N-K+1)/2,(N-K+3)/2,...,(N+K-1)/2]\}$$

\mathbf{KofN}_{DFT}^{LP} DFT -high-pass trimmed matrix $\mathbf{KofN}_{DFT}^{HP} = \left\{ \exp\left(i2\pi \frac{\tilde{k}\tilde{r}_{HP}}{N}\right) \right\}$

is a Vandermonde matrix, and, as such, it can be inverted

Theorem 2.

High-pass DFT band-limited signals of N samples with only K nonzero high frequency DFT coefficients can be precisely recovered from exactly K of their arbitrarily taken samples.

Analysis of transforms: DCT

DCT is an orthogonal transform with very good energy compaction properties. It is well suited for compressed representation of many types of signals

N -point Discrete Cosine Transform of a signal is equivalent to $2N$ -point Shifted Discrete Fourier Transform (SDFT) with shift parameters $(1/2,0)$ of the $2N$ - sample signal obtained from the initial one by its mirror reflection from its borders

K of N -trimmed matrix of $SDFT(1/2,0)$

$$\begin{aligned}\mathbf{KofN}_{SDFT} &= \left\{ \exp \left(i 2\pi \frac{(\tilde{k} + 1/2)\tilde{r}}{2N} \right) \right\} = \left\{ \exp \left(i 2\pi \frac{\tilde{k}\tilde{r}}{2N} \right) \left\{ \exp \left(i\pi \frac{\tilde{r}}{2N} \right) \delta(k-r) \right\} \right\} = \\ &= \mathbf{KofN}_{DFT} \left\{ \exp \left(i\pi \frac{\tilde{r}}{2N} \right) \delta(k-r) \right\}\end{aligned}$$

Therefore, for DCT theorems similar to those for DFT hold

Analysis of transforms: Discrete Fresnel transform

Canonical Discrete Fresnel Transform (***DFrT***) is defined as

$$a_k = \frac{1}{\sqrt{N}} \sum_{r=0}^{N-1} \alpha_r \exp \left[-i\pi \frac{(k\mu - r/\mu)^2}{N} \right]$$

where μ is a distance parameter.

DFrT can easily be expressed via DFT:

$$\alpha_r = \frac{1}{\sqrt{N}} \left\{ \sum_{k=0}^{N-1} \left[a_k \exp \left(i\pi \frac{k^2 \mu^2}{N} \right) \right] \exp \left(-i2\pi \frac{kr}{N} \right) \right\} \exp \left(i\pi \frac{r^2}{\mu^2 N} \right)$$

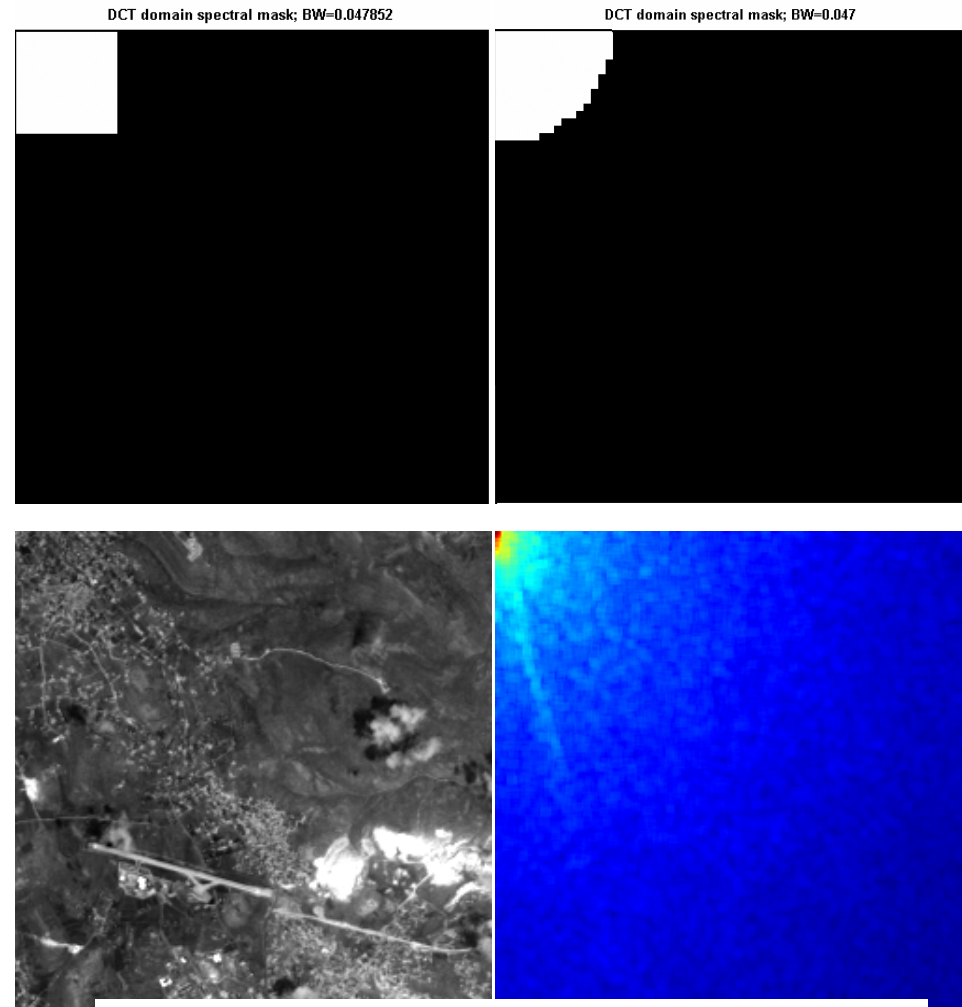
In a matrix form, it can be represented as a matrix product of diagonal matrices and the matrix of Discrete Fourier Transform. Therefore for Discrete Fresnel Transform formulation of band-limitation and requirements to positions of sparse samples are the similar to those for DFT.

2-D transforms:

- Separable band-limitation
- Inseparable band-limitation

Other transforms:

- Walsh transform
- Haar transform
- Wavelet transforms



Real life image and its DCT spectrum

Algorithms:

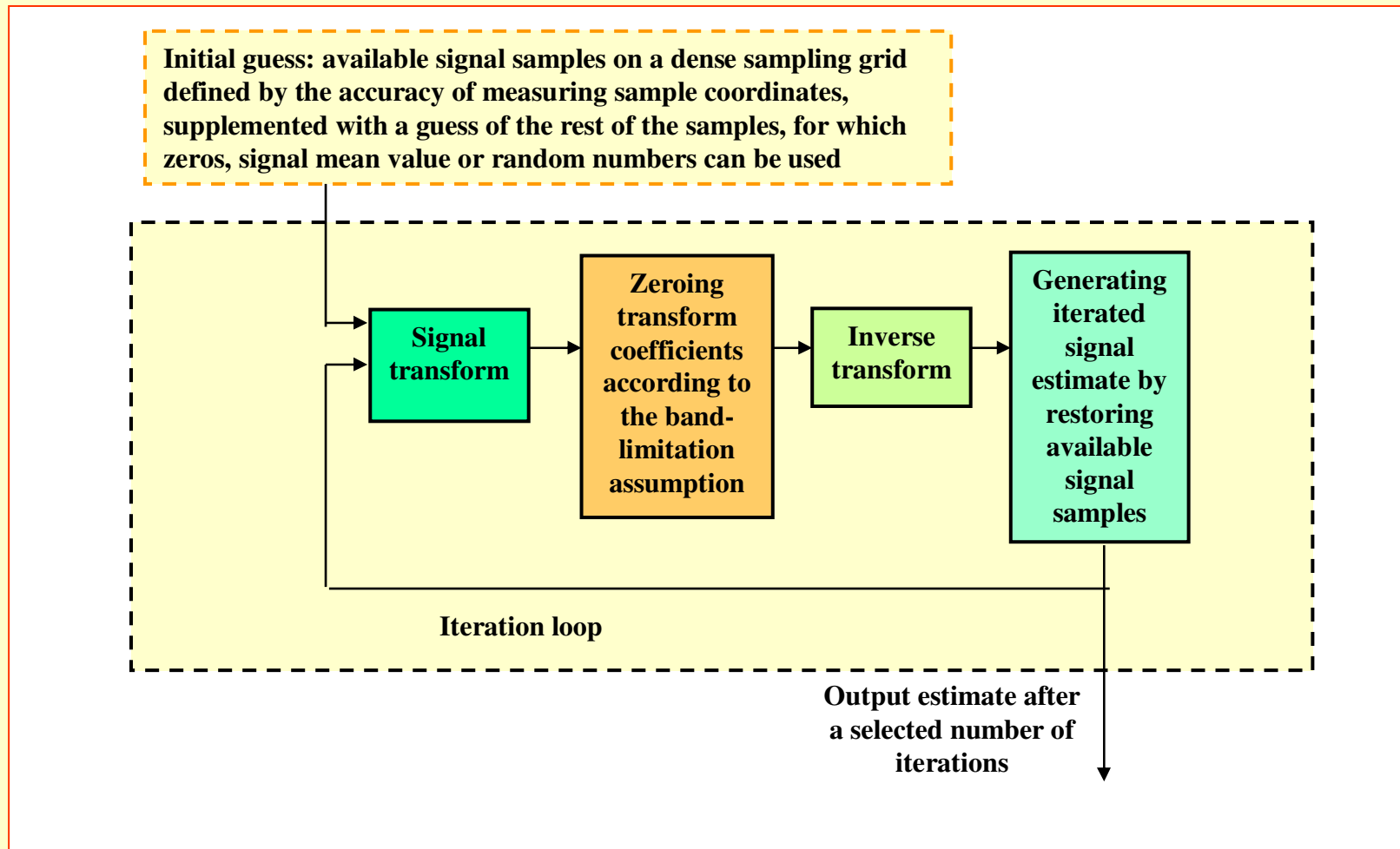
1. Direct matrix inversion $\hat{\mathbf{A}}_N^{BL} = \left\{ \hat{a}_k = \sum_{\tilde{r} \in \tilde{R}} [\mathbf{K} \text{of} \mathbf{N}_{\Phi}^{-1} \cdot \tilde{\mathbf{A}}_K] \phi_{\tilde{r}}(k) \right\}$

An open question: do fast algorithms for matrix inversion exist?

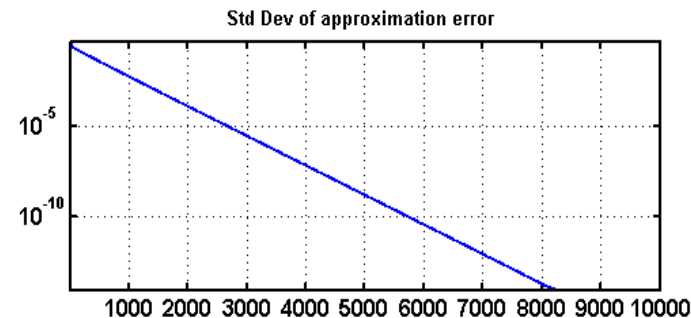
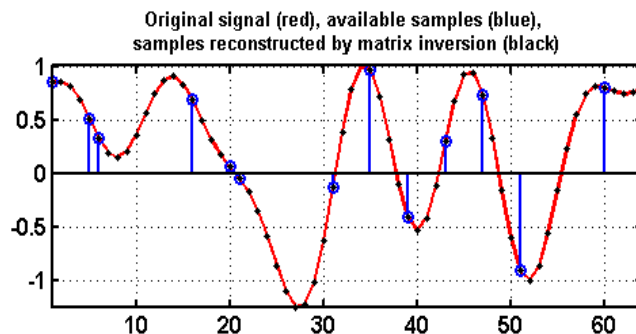
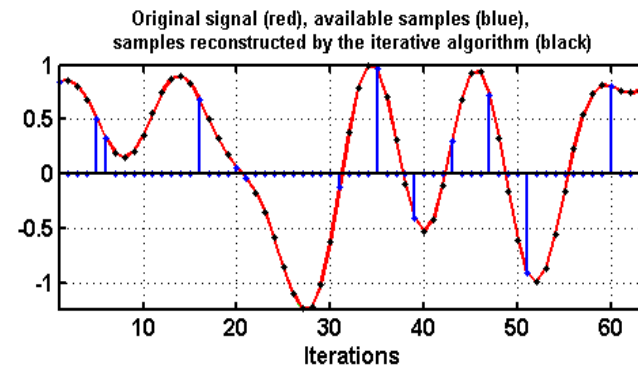
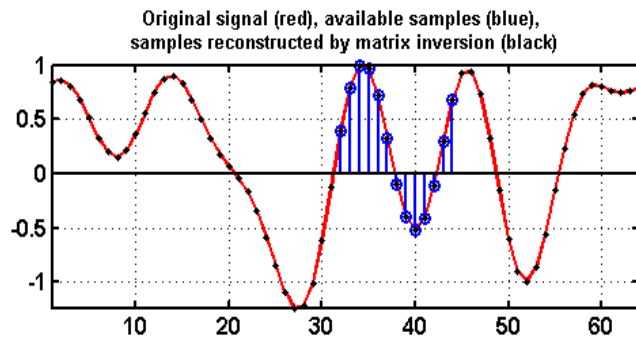
For DFT, DCT, Walsh, Haar and other transforms that feature FFT-type algorithms, pruned fast algorithms might be used.

2. Iterative Gershberg-Papoulis-type algorithm

Iterative Gershberg-Papoulis type signal recovery algorithm

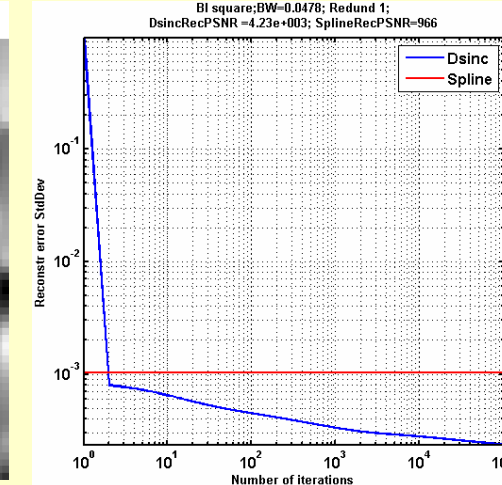
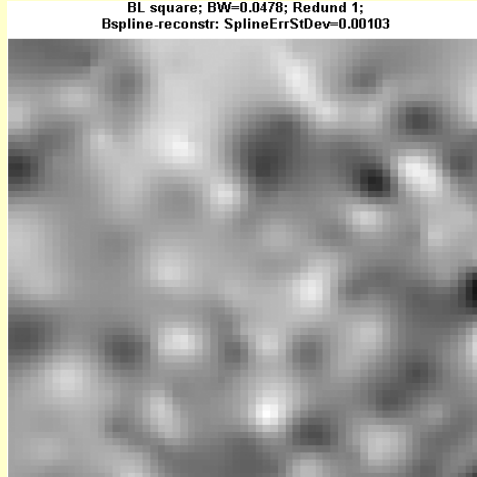
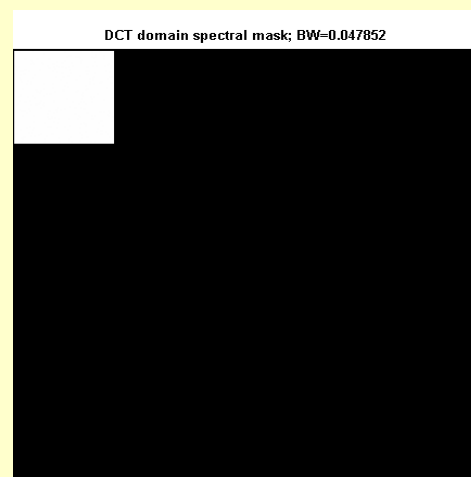
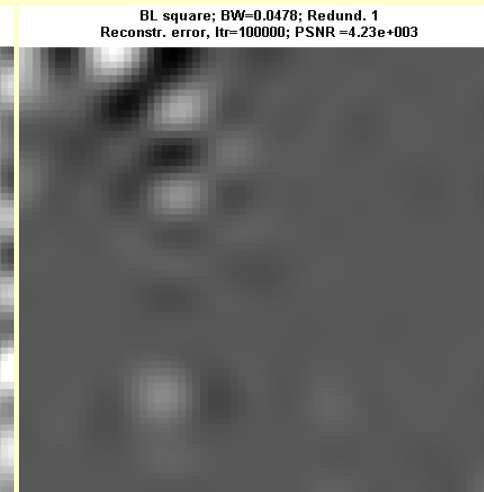
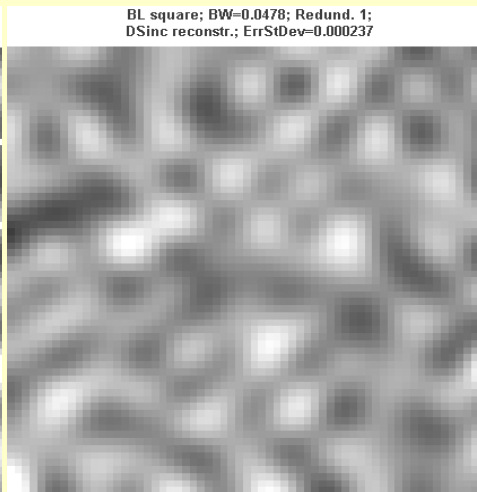
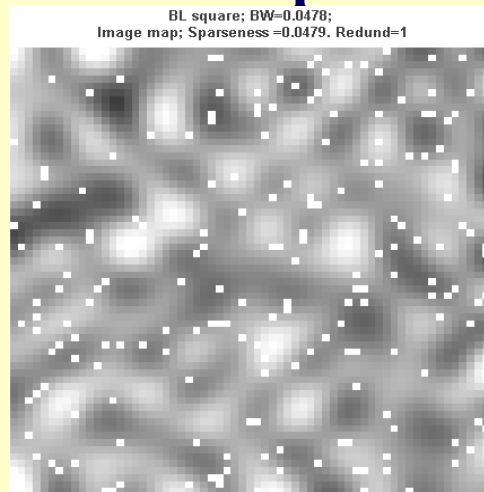


Experiments with DFT



Restoration of a DFT low pass band-limited signal by matrix inversion for the cases of random (a), upper) and compactly placed signal samples (a), bottom) and by the iterative algorithm (b). Bottom right plot shows standard deviation of signal restoration error as a function of the number of iterations. The experiment was conducted for a test signal length 64 samples; bandwidth 13 frequency samples ($\sim 1/5$ of the signal base band)

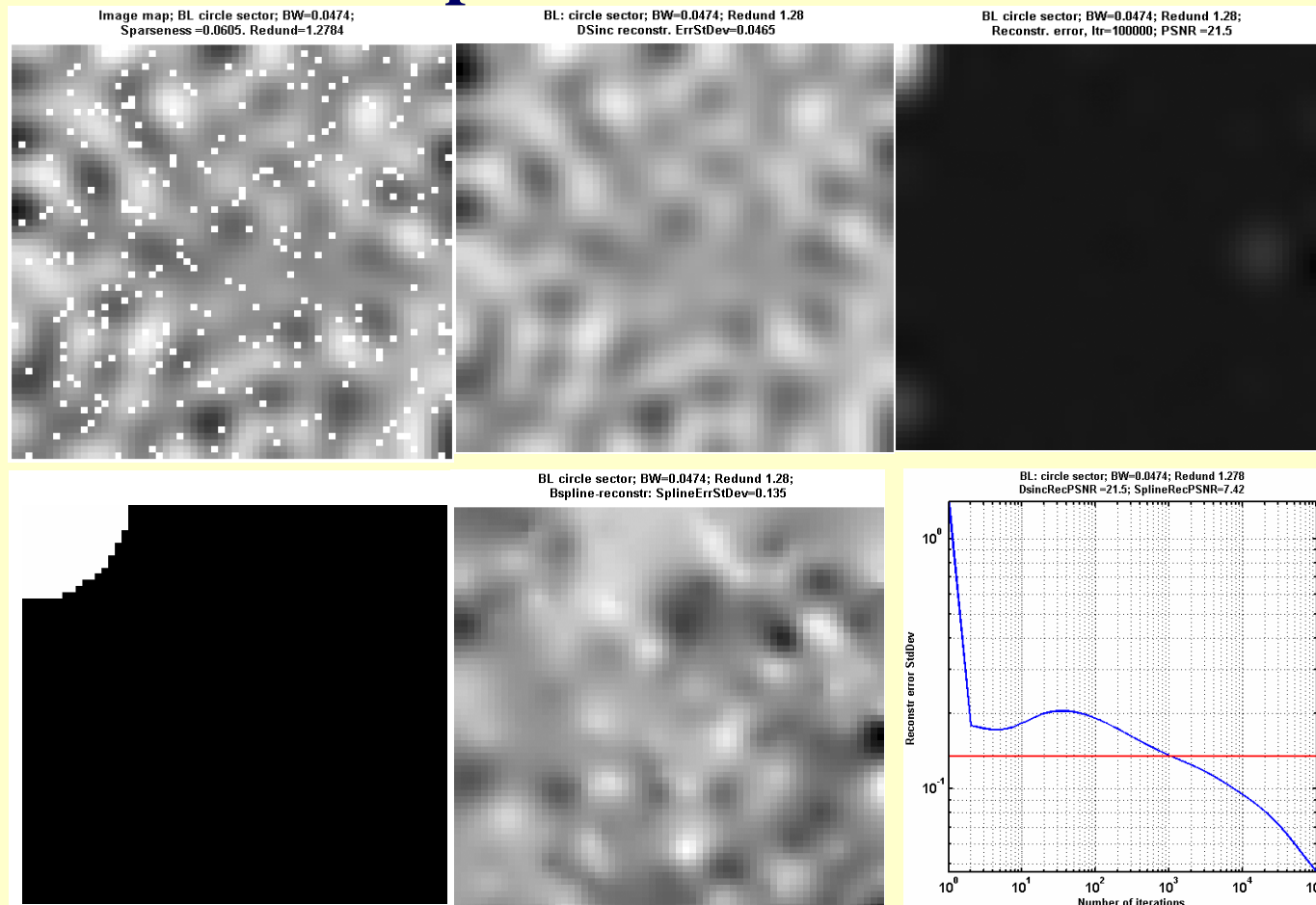
Image recovery from sparse samples: DCT with separable band limitation



Recovery of an image band limited in DCT domain by a square: a) – initial image with 3136 “randomly” place samples (shown by white dots); b) – the shape of the image spectrum in DCT domain; c) –image restored by the iterative algorithm after 100000 iterations with restoration PSNR (peak signal-to-error standard deviation) 4230; d) image restored by B-spline interpolation with restoration PSNR 966; e) iterative algorithm restoration error (white – large errors; black – small errors); f) –restoration error standard deviation versus the number of iterations for the iterative algorithm and that for the B-spline interpolation

[OUTIMG,t,t_r,StdErr,OUTIMG_spline, StdErr_spline,
msk]=map_reconstr_test_sinc_spline(64,0.05);

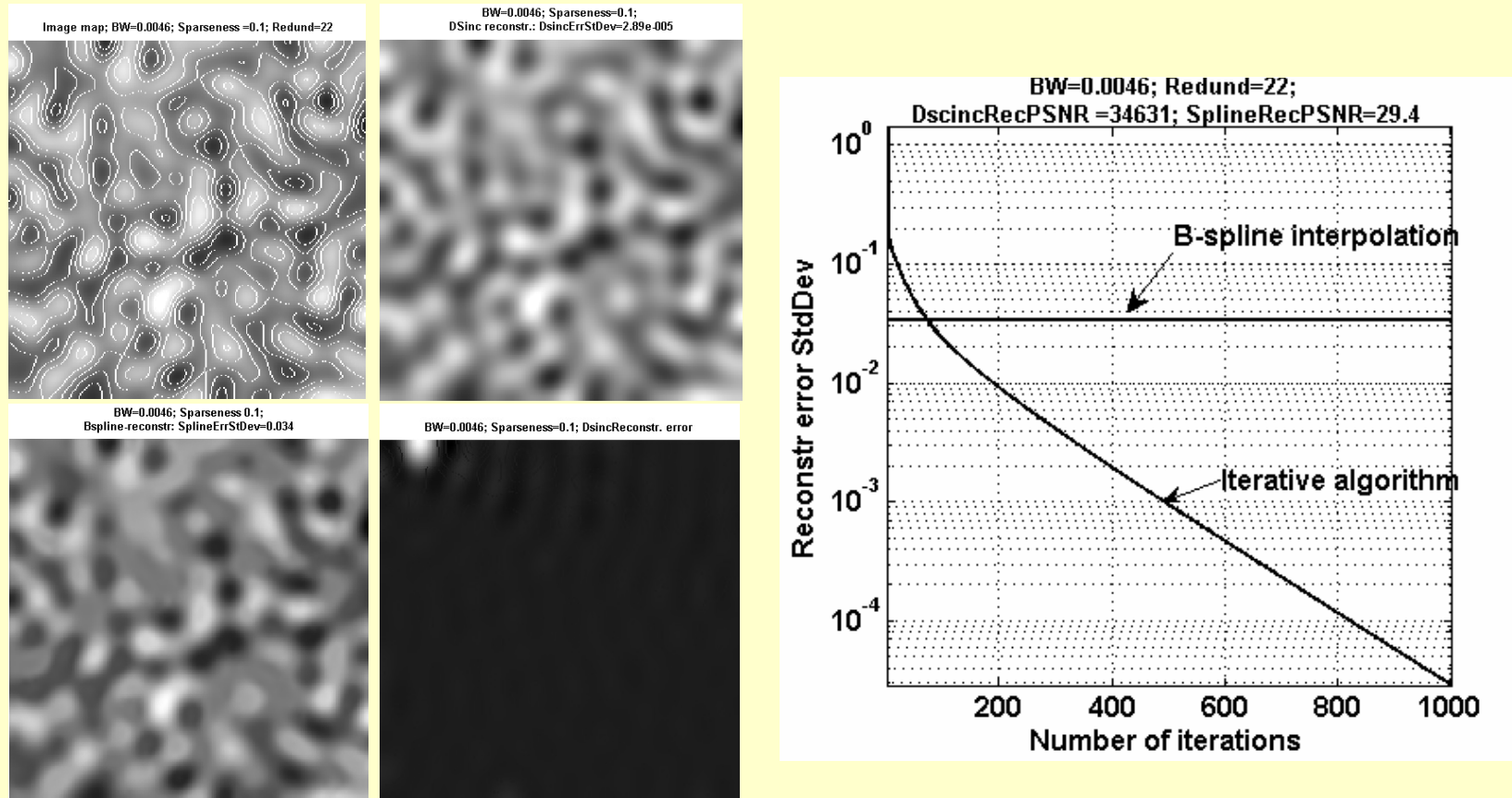
Image recovery from sparse samples: DCT with non-separable band limitation



Recovery of an image band limited in DCT domain by a circle sector: a) – initial image with 3964 “randomly” place samples (shown by white dots); b) – the shape of the image spectrum in DCT domain; c) –image restored by the iterative algorithm after 100000 iterations with restoration PSNR (peak signal-to-error standard deviation) 21.5; d) image restored by B-spline interpolation with restoration PSNR 7.42; e) iterative algorithm restoration error (white – large errors; black – small errors); f) –the restoration error standard deviation versus the number of iterations of the iterative algorithm and that for the B-spline interpolation

[OUTIMG,t,t_r,StdErr,OUTIMG_spline,StdErr_spline,msk]=map_reconstr_test_sinc_spline(64,0.05);

Image recovery from level lines: DCT with non-separable band limitation



Recovery of an image band limited in DCT domain by a circle sector from its level lines: a) – initial image with level lines (shown by white dots); b) –image restored by the iterative algorithm after 1000 iterations with restoration PSNR 3.5×10^4 (note that the restoration error is concentrated in a small area of the image); c) image restored by B-spline interpolation with restoration PSNR 29.4; d) iterative algorithm restoration error (white – large errors; black – small errors); e) –the restoration error standard deviation versus the number of iterations of the iterative algorithm and that for the B-spline interpolation

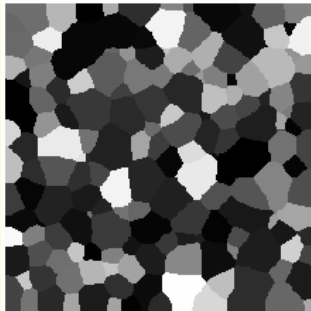
Signal recovery from sparse or non uniformly sampled data as an approximation task

Signal recovery from sparse or non-uniformly sampled data can be treated as finding best signal band-limited approximation. For this, the above theory and algorithms can be applied as following:

- 1. Given a certain number of available signal samples, specify the signal dense sampling grid and the required number of samples to be recovered.**
- 2. Select a transform with presumably better energy compaction capability for the signal at hand and specify the signal band limitation in the domain of this transform.**
- 3. Place available signal samples on the signal dense sampling grid and run the direct matrix inversion or the iterative reconstruction algorithm.**

Energy compaction capability of transforms

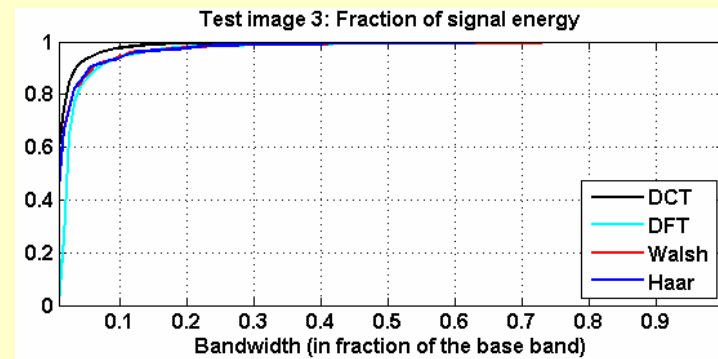
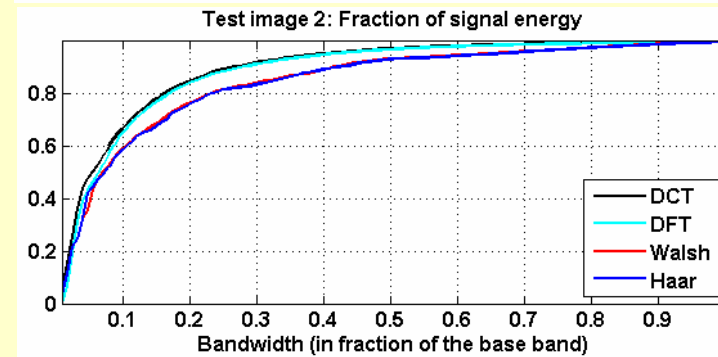
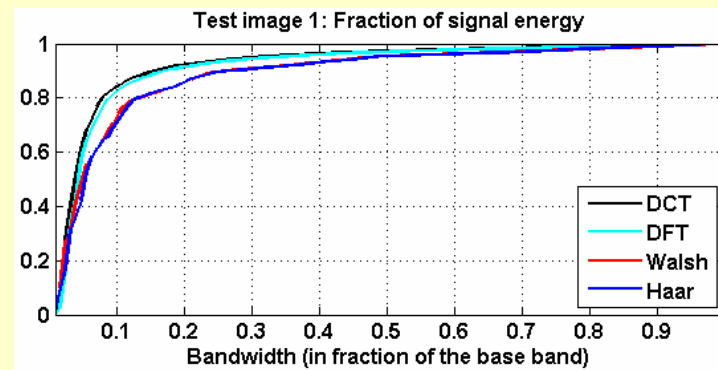
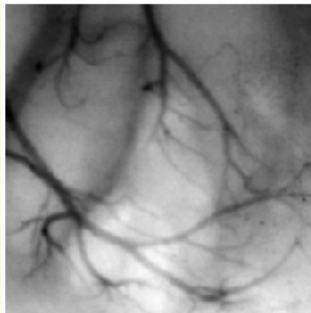
Test image 1



Test image 2

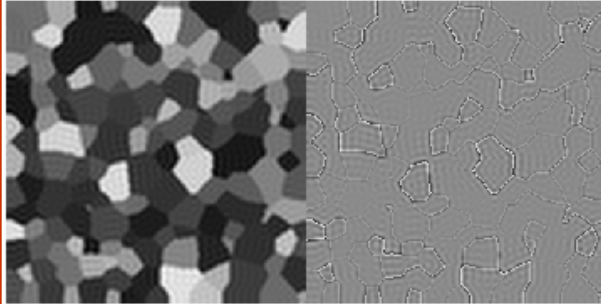


Test image 3

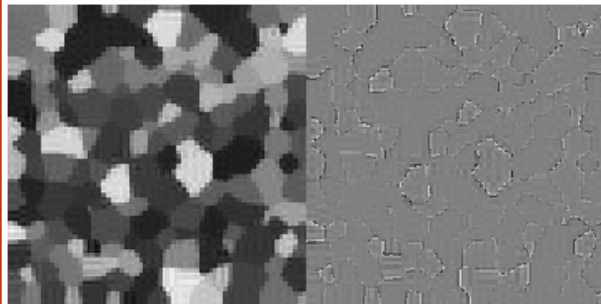


Errors due to image band limitation

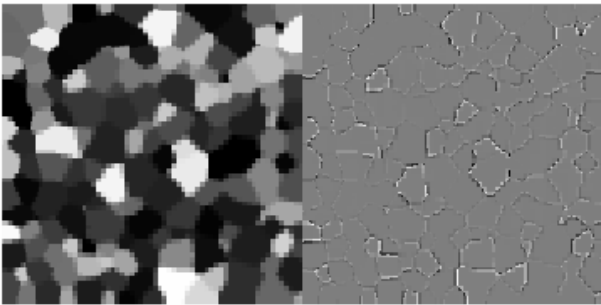
DCT_LP image; BW=0.3 ;StdErr=16.3692



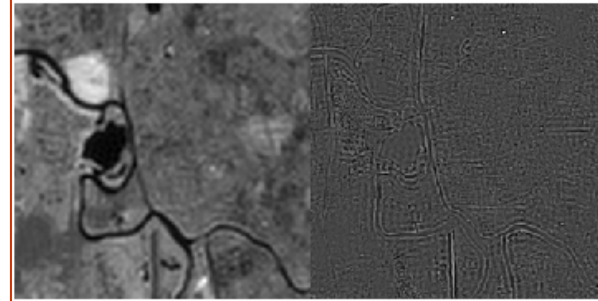
Walsh_LP image; BW=0.3 ;StdErr=22.1208



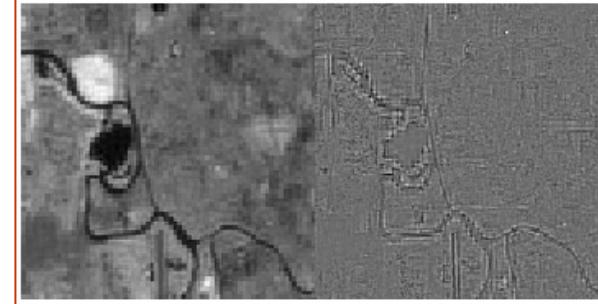
Haar_LP image; BW=0.3 ;StdErr=22.3649



DCT_LP image; BW=0.3 ;StdErr=2.9807



Walsh_LP image; BW=0.3 ;StdErr=4.1801



Haar_LP image; BW=0.3 ;StdErr=4.2585



Applications examples:

- image super-resolution from turbulent videos (shown above)**
- Image super-resolution in computed tomography**

Super-resolution in computed tomography

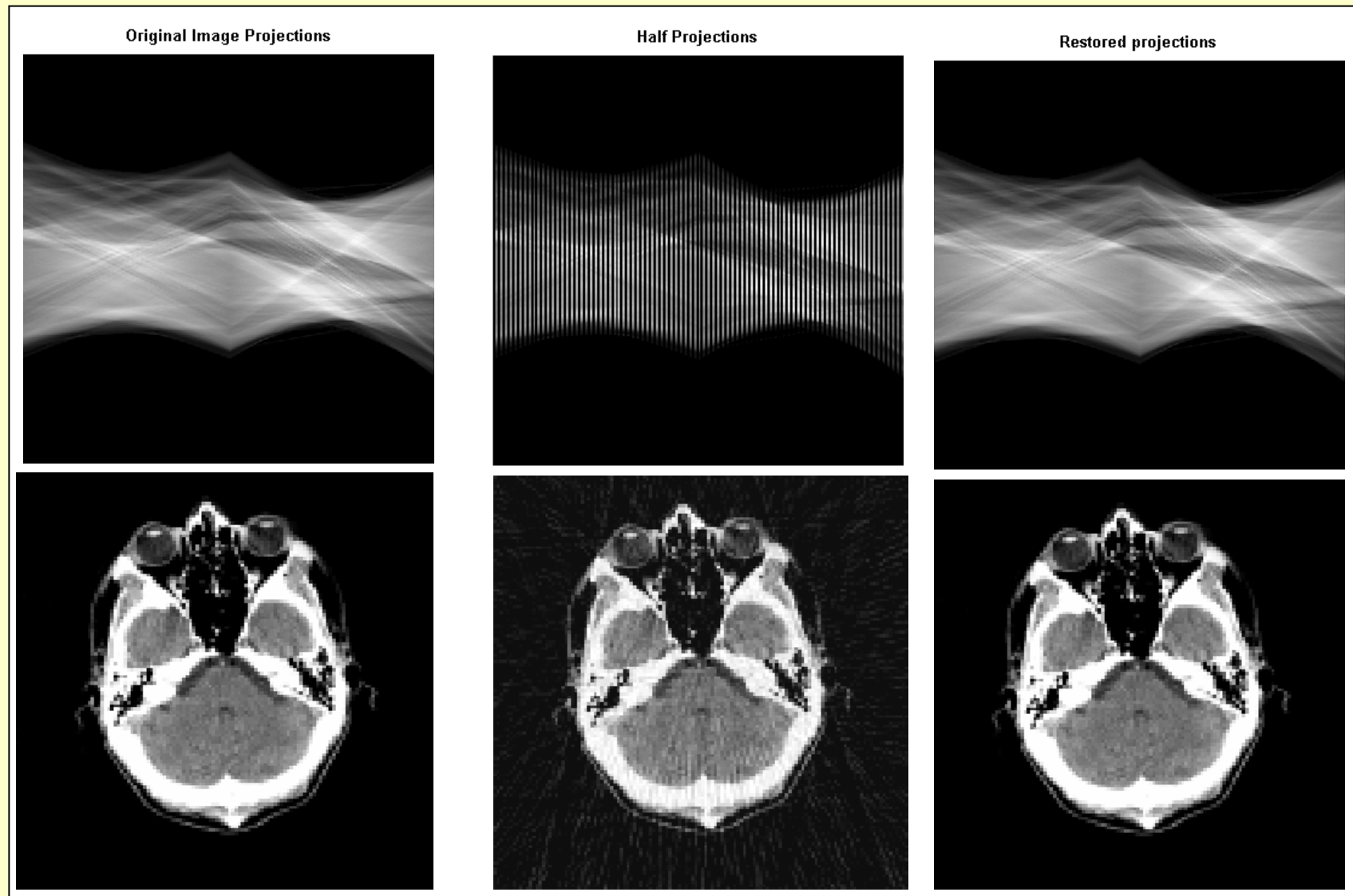


Image recovery from sparse samples: the “Compressing sensing” approach

Images sampling and redundancy

Fourier spectra of images are usually quite rapidly decaying with frequency f . However high frequency spectral components carry highly important information for image analysis, object detection and recognition that can't be neglected in spite of the fact that their contribution to signal

energy $\int_{-\infty}^{\infty} |a(x)|^2 dx = \int_{-\infty}^{\infty} |\alpha(f)|^2 df$ is relatively small. For this reason, sampling interval Δx must be taken sufficiently small in order to preserve image essential high frequencies. As a consequence, image representation by samples is frequently very redundant because samples are highly correlated.

This means, that, in principle, much less samples would be sufficient for image reconstruction if the reconstruction is done in a more sophisticated way than by means of conventional weighted summation according to the sampling theorem

Described methods for image recovery from sparse samples by means of their band-limited approximation in certain transform domain require explicit formulation of the desired band limitation in the selected transform domain.

This a priori knowledge that one has to invest is quite natural to assume. If one selects a transform according to its energy compaction capability, one may know how this capability works, i.e. what transform coefficients are expected to be zero or non-zero.

If, however, this is not known or not certain a priori, image recovery can be achieved using an approach, which obtained the name, in fact, quite confusing, “compressive sensing” (Donoho, D., “Compressed sensing”(2006), IEEE Trans. On Information Theory, v. 52(4), pp. 1289-1306).

The compressive sensing approach to signal reconstruction from sparse data

The “compressive sensing” approach also assumes obtaining band-limited, in certain selected transform domain, approximation of images but does not require explicit formulation of the band-limitation.

According to this approach, from available $M < N$ signal samples $\{a_{\tilde{m}}\}$, a signal $\{a_k\}$ of N samples is recovered that provides minimum to L_1 norm $\|\alpha\|_{L_1} = \sum_{r=0}^{N-1} |\alpha_r|$ of signal transform coefficients $\{\alpha_r\}$ for the selected transform.

The basis of this approach is the observation, that minimization of signal L_1 norm “almost always” in transform domain leads to minimization of L_0 – norm $\|\alpha\|_{L_0} = \sum_{r=0}^{N-1} |\alpha_r|^0$, that is to the minimization of the number of non-zero signal transform coefficients

The price for the uncertainty regarding band limitation is that the number of required signal samples M must be in this case redundant with respect to the given number K non-zero spectral coefficients: $M/K = O(\log N)$

**Sinc-lets and other discrete signals
sharply limited both in signal and
DFT/DCT domains**

The uncertainty principle:

Continuous signals cannot be both finite and sharply band-limited:

$$X_{\epsilon S} \times F_{\epsilon B} > 1$$

where $X_{\epsilon S}$ is interval in signal domain that contains ϵS - fraction of its entire energy, $F_{\epsilon B}$ is interval in Fourier spectral domain that contains ϵB - fraction of signal energy and both ϵS and ϵB are sufficiently small.

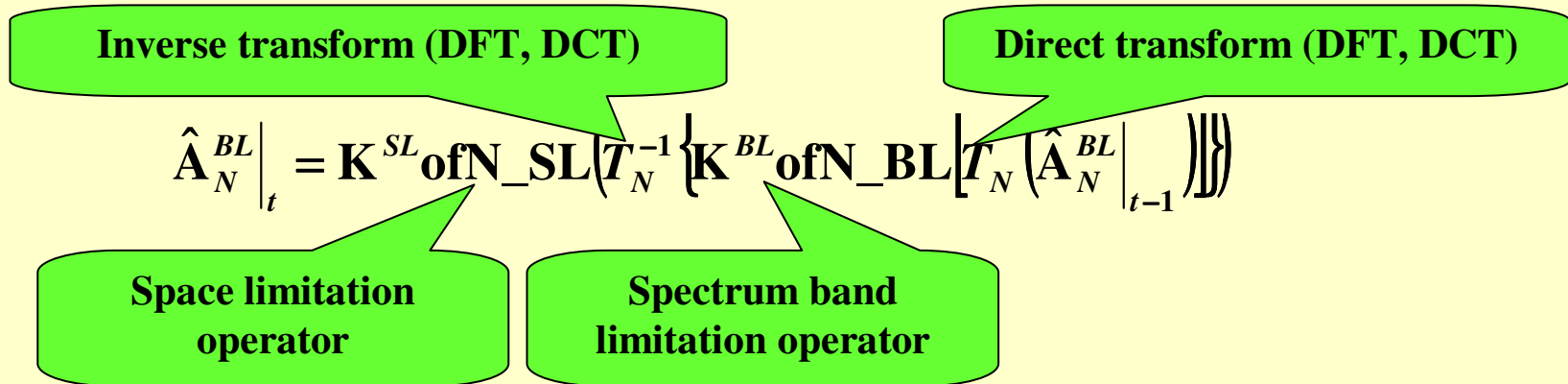
How the uncertainty principle can be translated to discrete signals?

- **Discrete signals that represent continuous signals through their samples are always finite as they contain finite number of samples.**
- **Discrete signals can be sharply “band-limited” in any transform, including DFT and DCT.**
- **For some transforms, such as, for instance, Haar transform and Radon Transform, discrete signals that are sharply limited both in signal and transform domain obviously exist**

Do exist discrete signals that are sharply limited both in signal and DFT or/and DCT, domains?

Space-limited & Band-limited discrete signals do exist

They are fixed points of the iterative algorithm:



Images

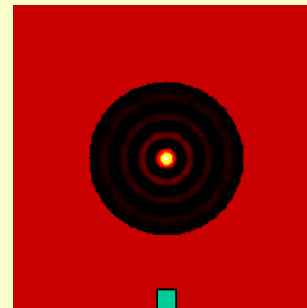
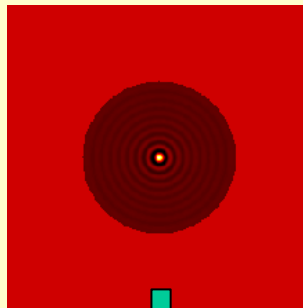
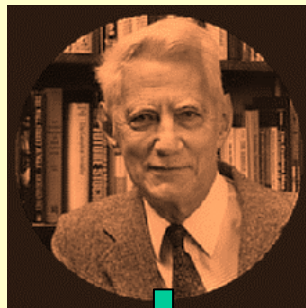
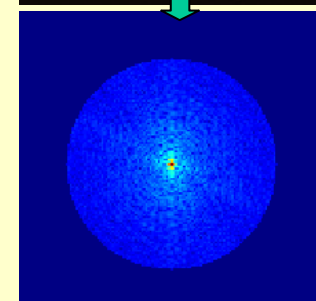
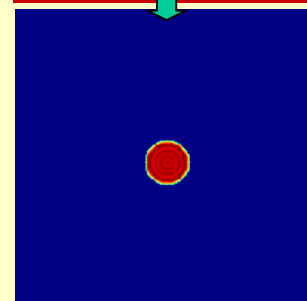
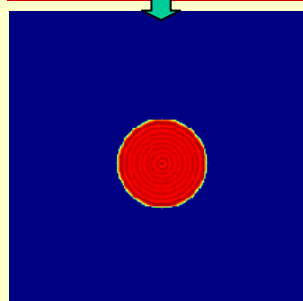
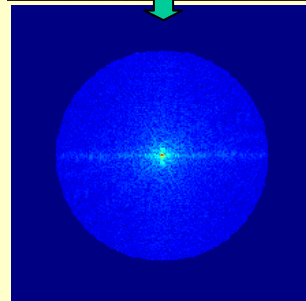


Image
DFT
spectra



The discrete uncertainty principle

The (continuous) uncertainty principle

$$X_{\varepsilon S} \times F_{\varepsilon B} > 1$$

Signal sampling interval

Signal sampling interval

$$N_{sign} \Delta x N_{spectr} \Delta f > 1$$

The number of signal non-zero samples

The number of signal non-zero samples

Cardinal sampling relationship

$$N_{sign} N_{spectr} > \frac{1}{\Delta x \Delta f}$$

$$\frac{1}{\Delta x \Delta f} = N$$

The number of signal samples

The discrete uncertainty relationship

$$N_{sign} N_{spectr} > N$$

Sinc-lets:

sharply band limited basis functions with
sharply limited support

$$SL_N^{BL} \Big|_{t=0} \delta(k - k_0)$$

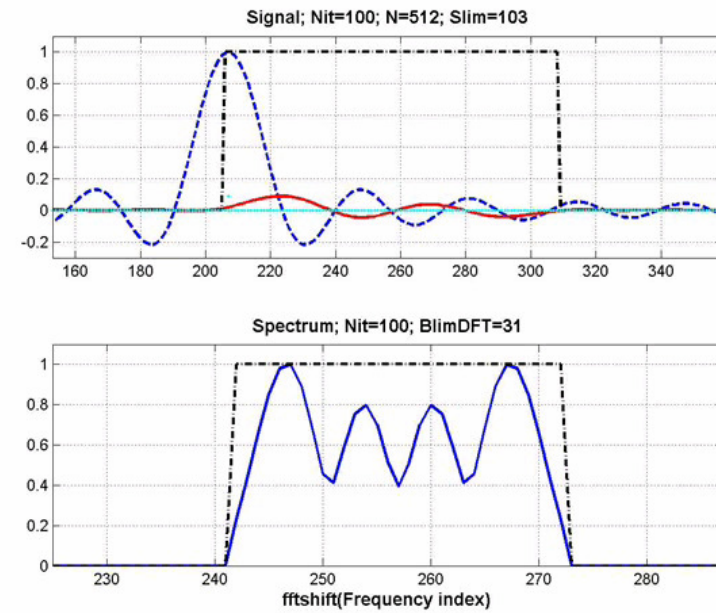
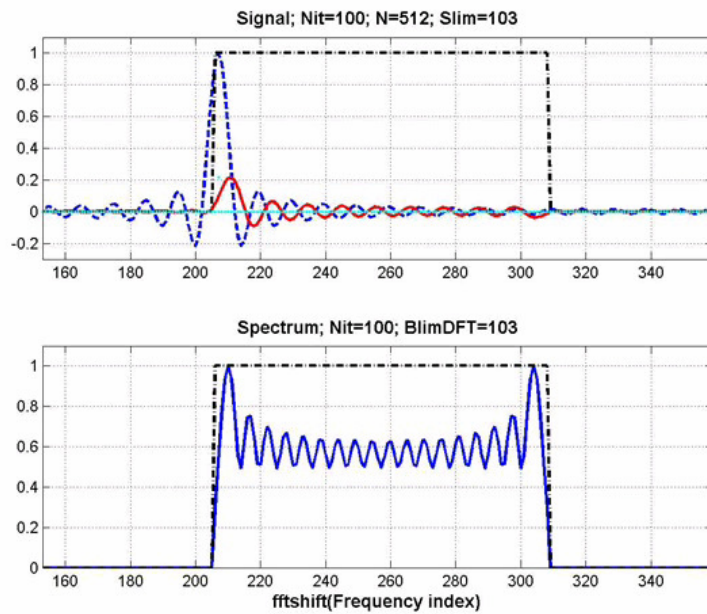
Inverse transform (DFT, DCT)

Direct transform (DFT, DCT)

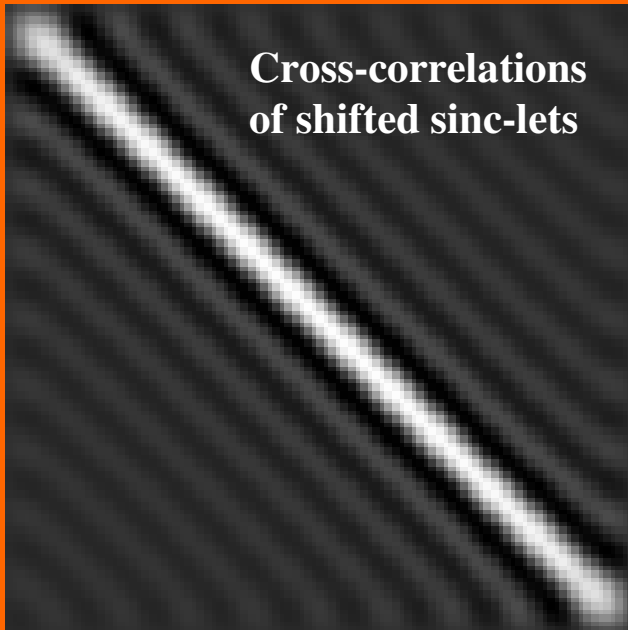
$$SL_N^{BL} \Big|_t = K^{SL} \text{ of } N_SL (T_N^{-1} \{ K^{BL} \text{ of } N_BL [T_N (SL_N^{BL} \Big|_{t-1})] \})$$

Space limitation
operator

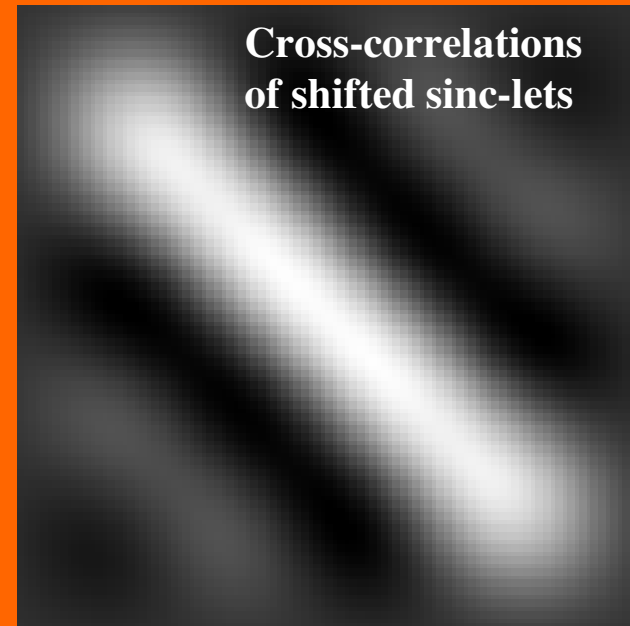
Spectrum band
limitation operator



**Cross-correlations
of shifted sinc-lets**

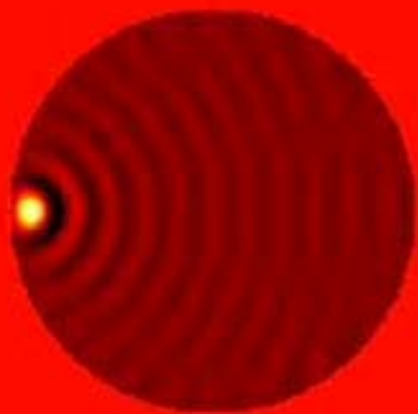


**Cross-correlations
of shifted sinc-lets**



2D Sinc-lets

Sinclets and Spectra; ResidStDev=0.00447; N=256; SzLim=128 ;Blim=51



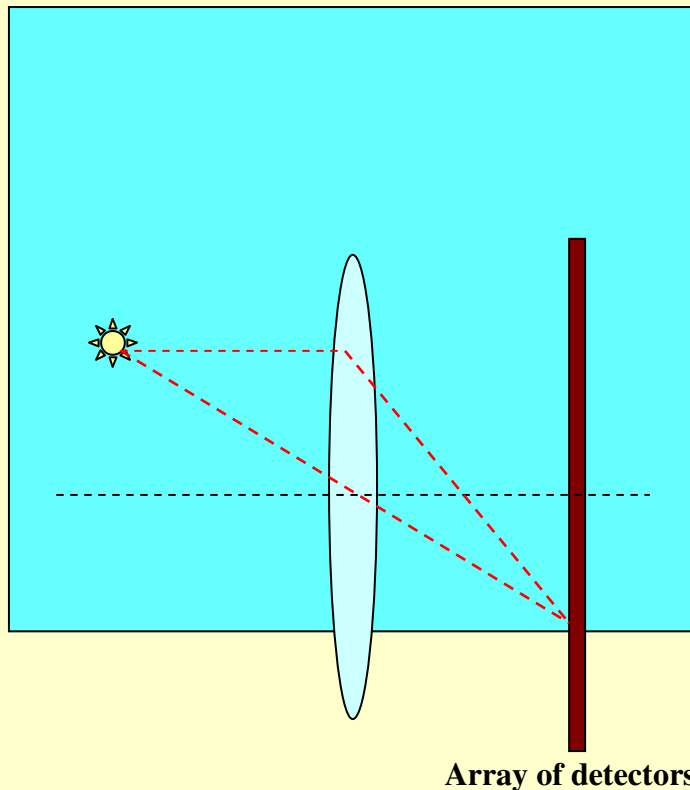
Imaging without optics : “Optics-Less Smart sensors”



telescope 9 m
mirror

Conventional optical imaging systems use photo-sensitive plane arrays of sub-sensors coupled with focused optics that form a map of the environment onto this image plane. The optics carry out all the information processing needed to form this mapping in parallel and at the speed of light, but comes with some disadvantages.

- **Because of the law of diffraction, accurate mapping requires large lens sizes and complex optical systems.**
- **Lenses limit the field of view and are only available within a limited range of the electromagnetic spectrum.**



Conventional optical imaging systems use photo-sensitive planar arrays of detectors coupled with focusing optics that form a map of the environment on the image plane. The optics carry this out at the speed of light, but lenses come with some disadvantages

- **Accurate mapping requires large lens sizes and complex optical systems.**
- **Lenses limit the field of view and**
- **Lenses are only available within a limited range of the electromagnetic spectrum.**

The ever-decreasing cost of computing makes it possible to make imaging devices smaller by replacing optical and mechanical components with computation.

Conventional optical imaging systems use photo-sensitive planar arrays of detectors coupled with focused optics that form a map of the environment on the image plane.

Optics carry this out at the speed of light, but come with some disadvantages.

- accurate mapping requires large and heavy lenses**
- lenses limit the field of view**
- lenses are not available for many types of radiation.**

The ever decreasing cost of computing and ever increasing computer power makes it possible to replace in imaging devices optical and mechanical components with computation.

This motivates a search for optics-less computational imaging devices.

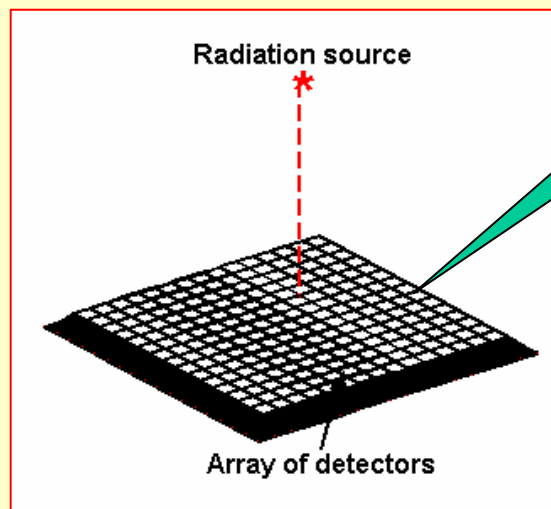
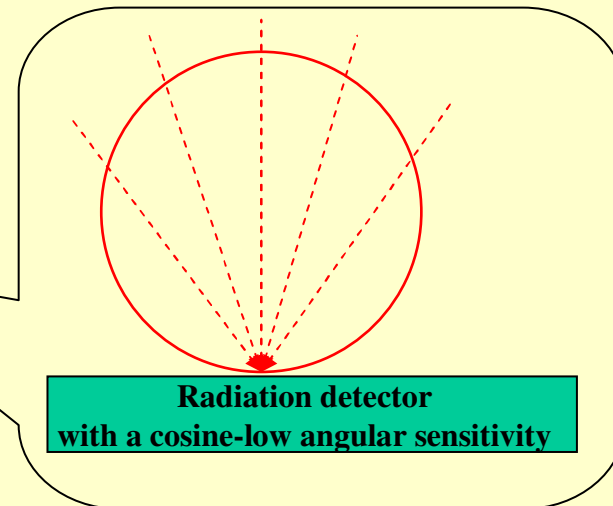
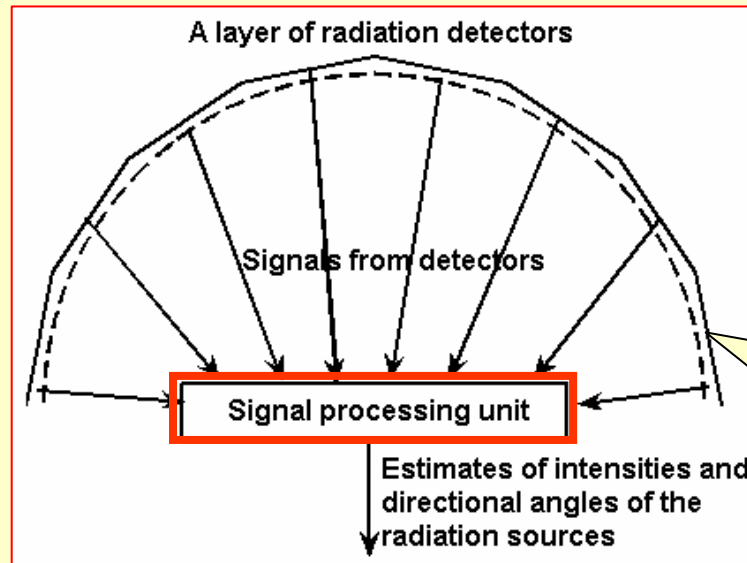
We treat images as data that indicate locations in space and intensities of sources of radiation and show that imaging tasks can be performed by means of optics less imaging devices consisting of set of bare radiation detectors arranged on flat or curved surface and supplemented with signal processing unit that use detector outputs to compute optimal statistical estimations of sources' intensities and coordinates.

We call this class of sensors

“Optics-Less Smart” (OLS) sensors

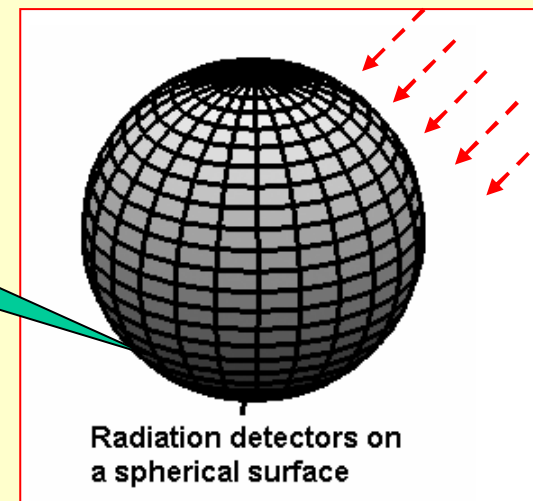
Optics-less radiation sensors:

arrays of radiation detectors with natural cosine-law or alike angular sensitivity arranged on flat or curved surfaces and supplemented with a signal processing unit



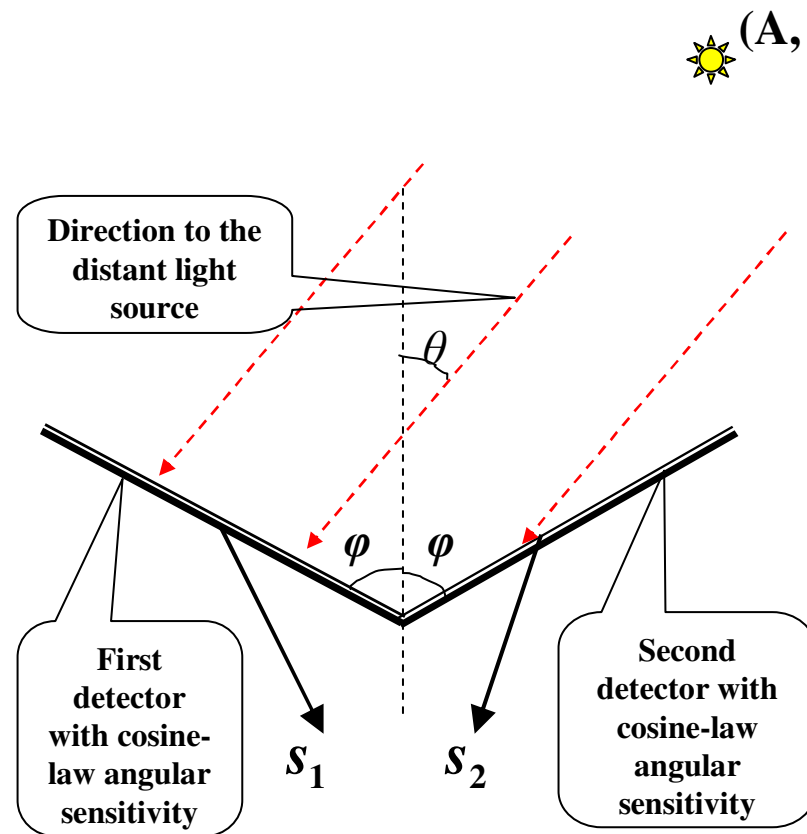
Planar model

Spherical model



Examples of the physical design and models used in experiments

An outline of the basic idea: Locating a single distant radiation source (planar model)



MAP
estimates:

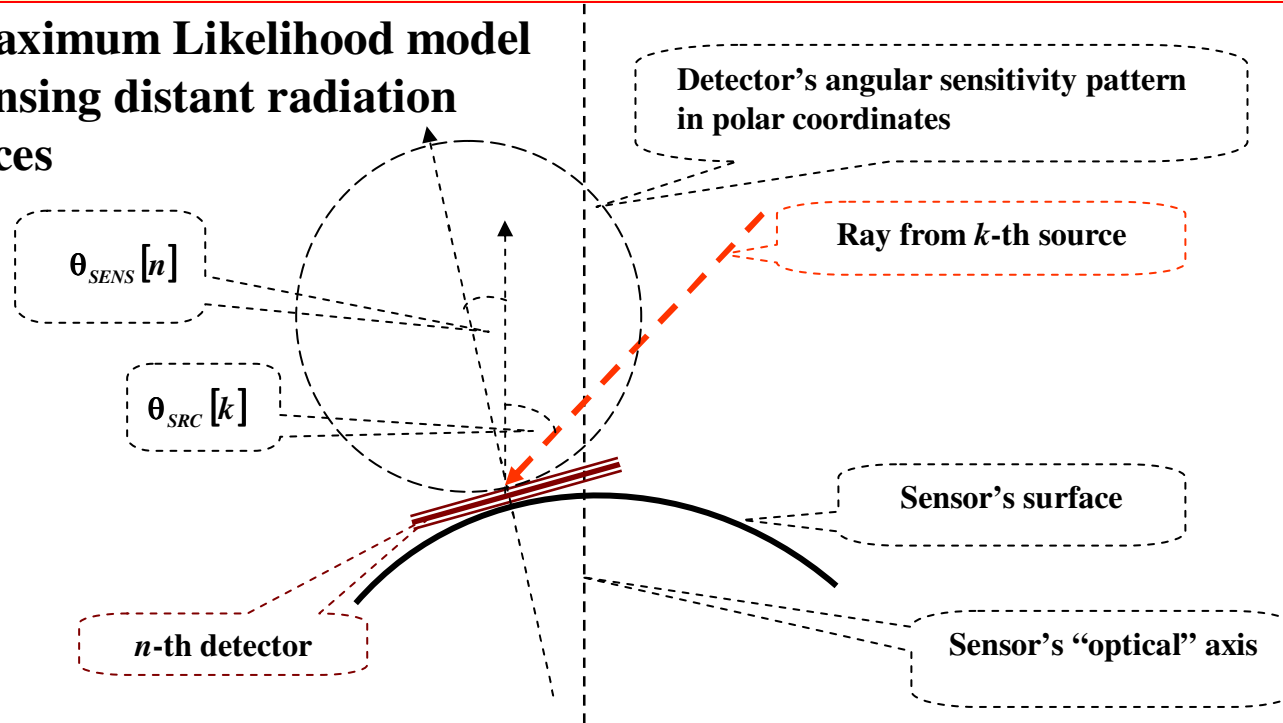
$$\hat{A} = \frac{\sqrt{s_1^2 + s_2^2 + 2s_1s_2 \cos 2\varphi}}{\sin 2\varphi}$$

$$\tan \hat{\theta} = \frac{s_1 - s_2}{s_1 + s_2} \tan \varphi$$

Sensor's operation principle:

generating, using signals from all elemental detectors, optimal statistical estimates of the radiation source intensity and coordinates or directional angles

**A Maximum Likelihood model
of sensing distant radiation
sources**



$$s[n] = \sum_{k=1}^K I[k] \text{AngSens}(\theta_{SRC}[k] + \theta_{SENS}[n]) + v[n]$$
$$\{\hat{I}[k], \hat{\theta}_{SRC}[k]\} = \arg \min_{\{I[k], \theta_{SRC}[k]\}} \left\{ \sum_{n=1}^N \left(s[n] - \sum_{k=1}^K I[k] \text{AngSens}(\theta_{SRC}[k] + \theta_{SENS}[n]) \right)^2 \right\}$$

Performance evaluation: theoretical lower bounds. Spherical sensor, single distant source

- OLS sensors are essentially nonlinear devices that can't be described in terms of point-spread functions. Their performance can be characterized by the probability distribution function of source parameter estimation errors
- Statistical theory of parameter estimation shows that, for parameter estimation from data subjected to sufficiently small independent Gaussian additive noise, estimation errors have a normal distribution with mean of zero and standard deviation given by the Cramer-Rao lower bound (CRLB)

Assuming the simplest **Lambertian cosine law angular sensitivity function** of the detectors

$$\text{AngSens}(\vartheta) = \begin{cases} \cos \vartheta, & |\vartheta| < \pi/2 \\ 0, & |\vartheta| \geq \pi/2 \end{cases}$$

CRLBs are found, for a single source and for the spherical model, to be

$$\sqrt{\text{var}\{\hat{\theta}_{SRC}\}} \geq \frac{2\sigma}{\sqrt{N}I}; \quad \sqrt{\text{var}\{\hat{I}\}} \geq \frac{2\sigma}{\sqrt{N}}$$

where σ is standard deviation of detector's noise; N is the number of detectors, I is the source intensity

Performance evaluation: theoretical lower bounds. Spherical sensor, two and more sources:

For the case of two sources, CRLBs are found to be

$$\sqrt{\text{var}\{\hat{\theta}_{SRC}[k]\}} = \frac{2\sigma}{I[k]\sqrt{\Delta\theta_{SRC}/\Delta\theta_{SENS}}}; \text{ given } \Delta\theta_{SRC} > \Delta\theta_{SENS}; k = 1, 2$$

where $\Delta\theta_{SRS}$ is the angular difference between sources and $\Delta\theta_{SENS}=\pi/N$ is the angle between neighboring detectors.

Resolving power of the sensor:

If the angular separation between sources is smaller than the angular separation between neighboring detectors ($\Delta\theta_{SENS} > \Delta\theta_{SRS}$), the estimator's performance rapidly worsens and becomes no better than that of random guessing.

Numerical results for cases with more than two sources show that regardless of the number of equally-spaced sources, the average estimation error for all the sources is equal to the error predicted for the 2-source problem

Optics Less sensor basic operation modes

- "General localization" mode: localization and intensity estimation of a given number of radiation sources.**
- "Constellation localization" mode: estimation of intensities and locations of "constellations" of radiation sources, which consist of a known number of point sources of known configuration and relative distribution of intensities**
- "Imaging" mode: estimation of intensities of a given number of radiation sources in the given locations, for instance, on a regular grid.**

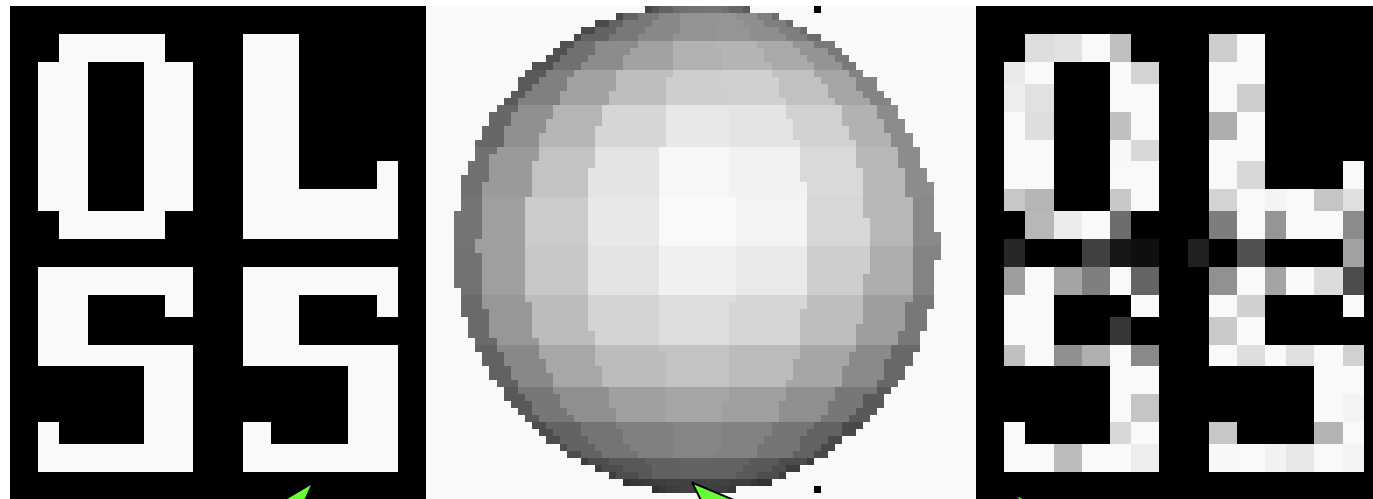
Computer model:

Spherical and planar models of optics less radiations sensors were tested in the localization and imaging modes by numerical simulation using, for generating Maximum Likelihood estimates of sources' intensities and locations, the multi-start global optimization method with pseudo-random initial guesses and Matlab's quasi-Newton method for finding local optima.

In order to improve reliability of global maximum location and accelerate the search, input data were subjected to decorrelation preprocessing by means of the “whitening” algorithm that proved to be optimal preprocessing algorithm for point target location in clutter. It is interesting to note that a similar data decorrelation is known in vision science as “**lateral inhibition**”

Experiment:

Spherical sensor in the imaging mode

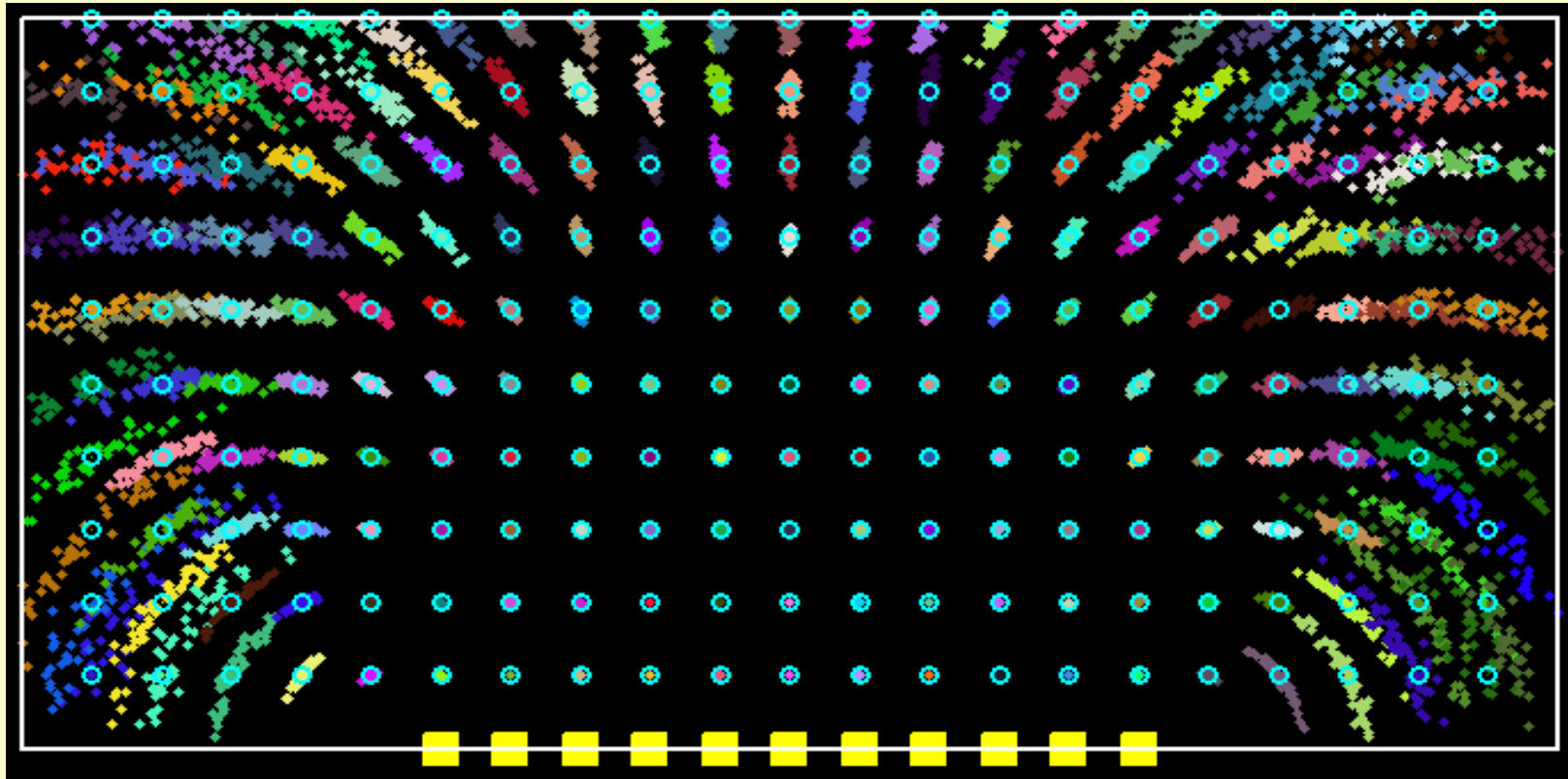


Pattern of 19x16 sources

Pattern of detectors' outputs
(spherical array of $16 \times 20 = 320$ detectors arranged within spatial angles $\pm\pi/2$ longitude and $\pm\pi/2.05$ latitude; detector's noise standard deviation 0.01)

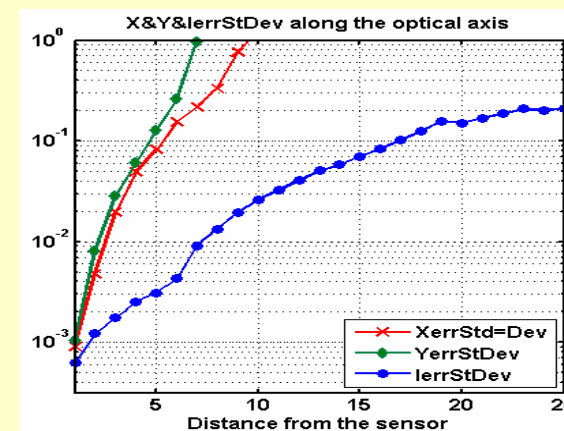
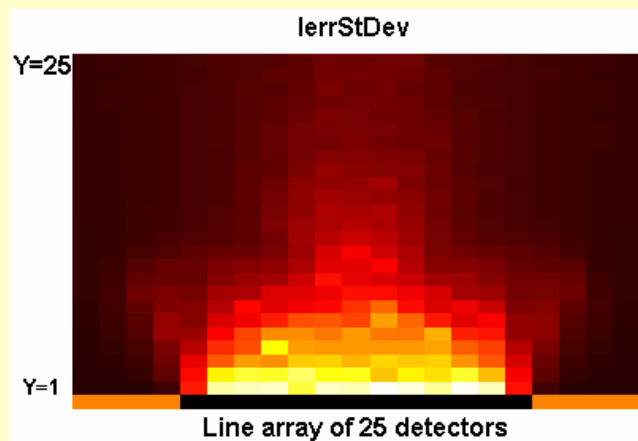
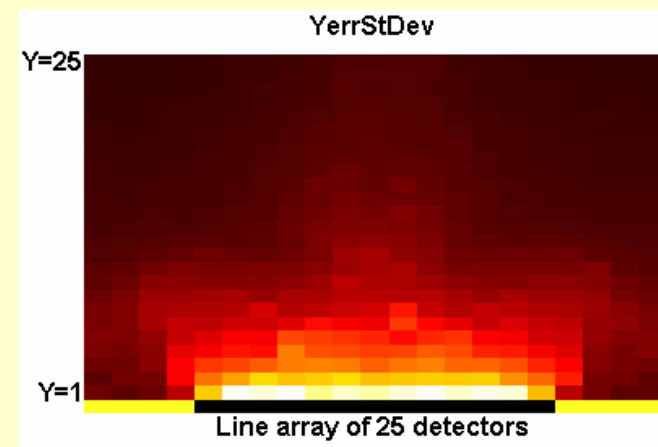
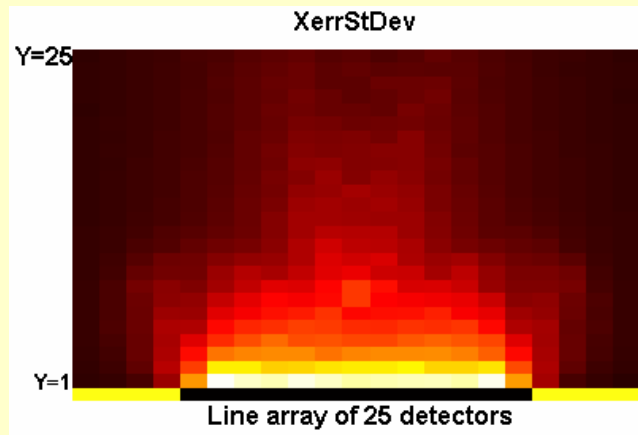
Reconstructed image
Standard deviation of estimation errors 0.064

Planar sensor in the localization mode



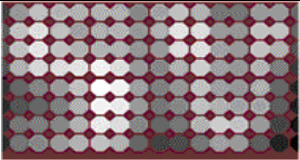

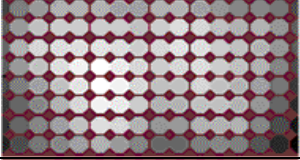

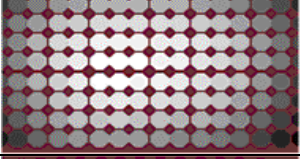
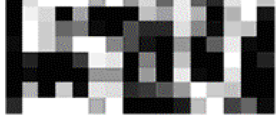
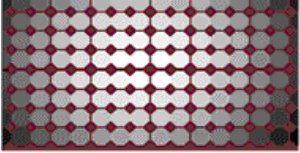
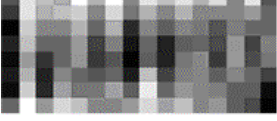
Spread of “hits” (color dots) of estimation of a single radiation source locations in different positions (marked by blue circles) with respect to the sensors, consisting of 11 detectors (yellow boxes)

Planar sensor in the localization mode: estimation errors of position and intensity of a single radiation source placed in different positions in front of the sensor



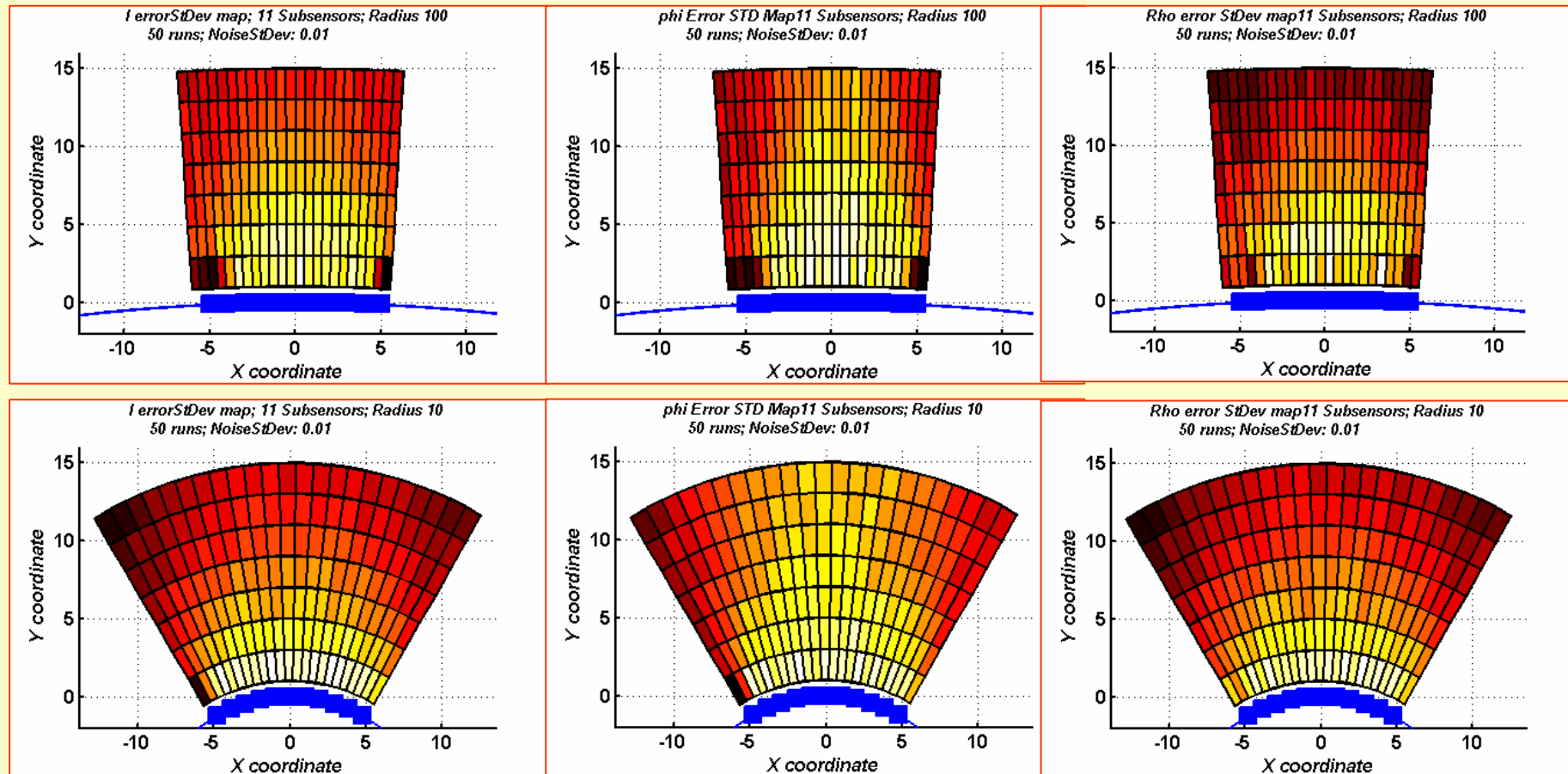
Maps of standard deviations of estimation errors of X-Y coordinates (a, b) and of intensity (c) of a radiation source as a function of the source position with respect to the surface of the line array of 25 detectors. Darker areas correspond to larger errors. Plot d) shows standard deviations of X, Y and intensity estimation errors as function of the distance from the sensor along the sensor 'optical axis' (central sections of Figs. a)-c))

Planar sensor in the imaging mode

Distance	Detector readings	Estimated source intensities
Z=1		 Error standard deviation 5.6850e-04
Z=2		 Error standard deviation 0.0105
Z=4		 Error standard deviation 0.0590
Z=8		 Error standard deviation 0.1197

Sensing of 8x16 radiation sources arranged on a plane in form of characters “SV” by a 3-D model of a flat OLS sensor of 8x16 elementary detectors in the “imaging” mode for distances of sources from the sensor Z=1 to 8 (in units of inter-detector distance). SNR was kept constant at 100 by making the source amplitude proportional to the distance between the source plane and sensor plane. Detector noise StDev=0.01.

Sensors on convex surfaces in the localization mode

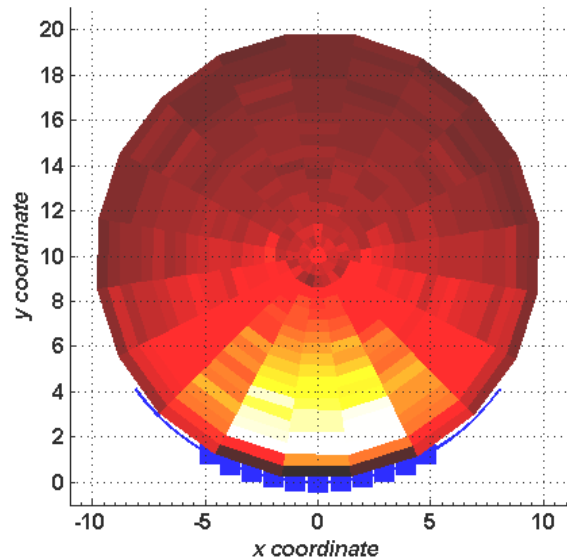


Sensors on bent convex surfaces (1D model, 11 detectors, noise standard deviation 0.01): map of standard deviations of estimation errors of source intensity (left column), that of source direction angle (central column) and that of the distance to the source (right column) as functions of the source position with respect to the sensor's surface. Darker areas correspond to larger errors.

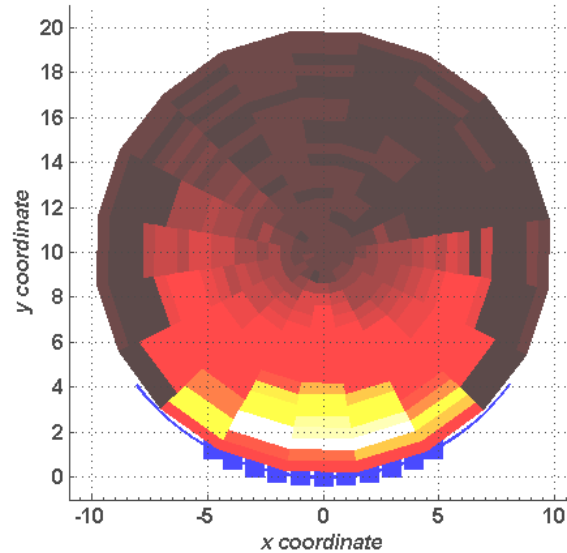
Sensors on concave surfaces in the localization mode

map_err_std_polar.m

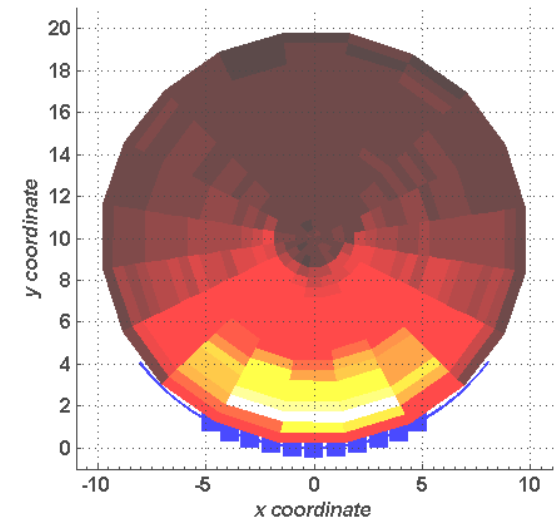
I-error STD Map; 11 Sensors; Radius of Bending: 10
Number of Noise Realizations: 50; NoiseSTD: 0.01



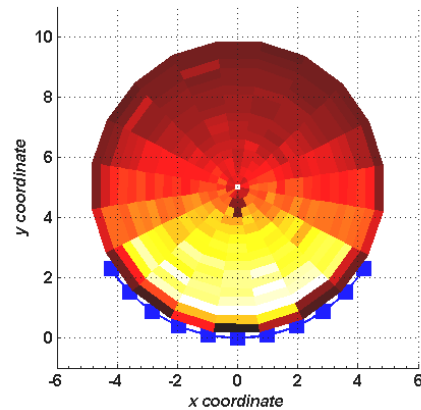
Phi-error STD Map; 11 Sensors; Radius of Bending: 10
Number of Noise Realizations: 50; NoiseSTD: 0.01



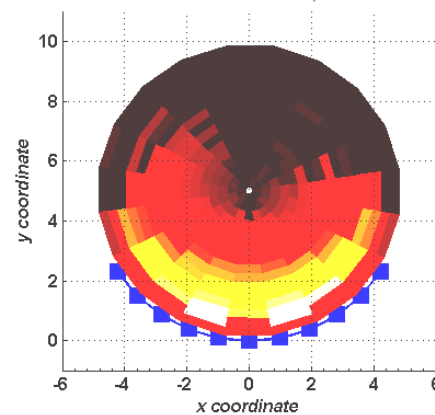
Rho-error STD Map; 11 Sensors; Radius of Bending: 10
Number of Noise Realizations: 50; NoiseSTD: 0.01



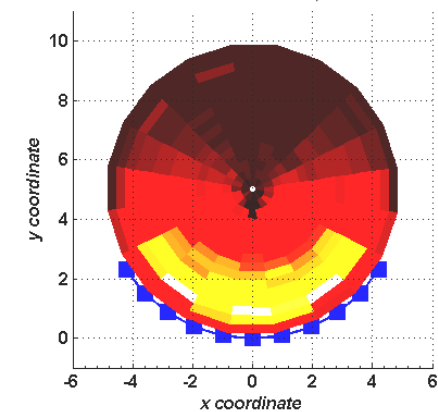
I-error STD Map; 11 Sensors; Radius of Bending: 5
Number of Noise Realizations: 50; NoiseSTD: 0.01



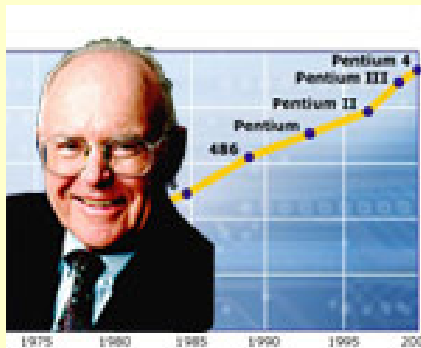
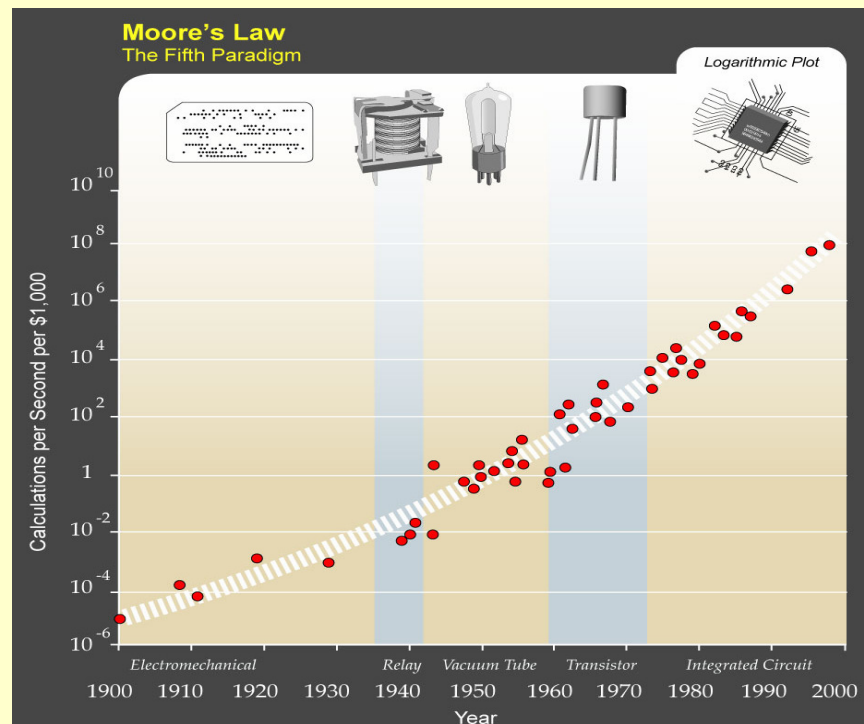
Phi-error STD Map; 11 Sensors; Radius of Bending: 5
Number of Noise Realizations: 50; NoiseSTD: 0.01



Rho-error STD Map; 11 Sensors; Radius of Bending: 5
Number of Noise Realizations: 50; NoiseSTD: 0.01



Optics-less “smart” sensors: advantages and limitations



Advantages

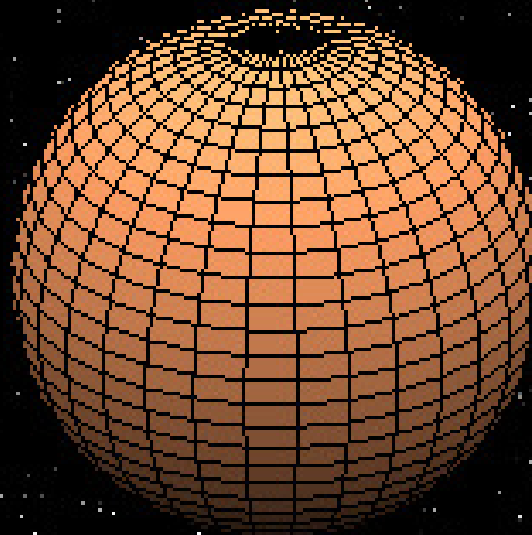
- No optics are needed, making this type of sensor applicable to virtually any type of radiation and to any wavelength
- The angle of view (of spherical sensors) is unlimited
- The resolving power is determined ultimately by the sub-sensor size, and not by diffraction-related limits
- Sensors without optics can be made more compact and robust than traditional optical sensors

Limitations:

High computational complexity, especially when good imaging properties for multiple sources are required.

However, the inexorable march of Moore's law makes such problems more feasible each year. Furthermore, the computations lend themselves to high-concurrency computation, so the computational aspects are not expected to hinder usage of OLS sensors.

A little imagination: a flying sighted brain



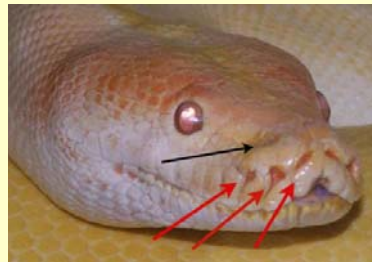
The background of the slide is a light-colored, marbled paper with a complex, organic pattern of veins in shades of beige, cream, and light brown.

COMPUTATIONAL IMAGING AND EVOLUTION OF VISION IN THE NATURE

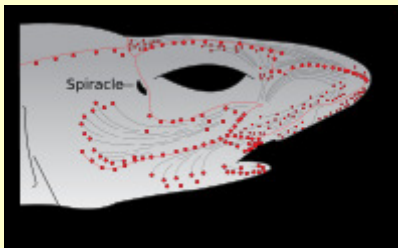
Optics-less extra ocular cutaneous (skin) vision in Nature



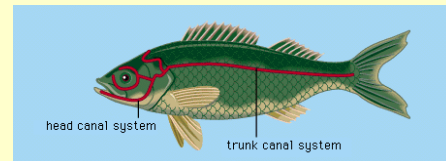
The flat worm has "cup" eyespots that can slightly distinguish light direction.



Pit organs in python. Arrows pointing to the pit organs are red; a black arrow points to the nostril



Electroreceptors and lateral line canals in sharks in some types of fish.



- Heliotropism of some plants
 - Eye spots (patches of photosensitive cells on the skin), cup eyes, and pit eyes
 - Cutaneous photoreception in reptiles
 - Infra-red radiation sensitive "pit organs" of vipers
 - The pressure sensitive "lateral line system" of fish, which they use to localize sources of vibration located within approximately one body length
 - Electric field sensitive receptors in sharks and in some types of fish, which allow animals to sense electrical field variations in their surroundings within approximately one body length
- There are also a number of reports on the phenomenon of primitive cutaneous vision in humans

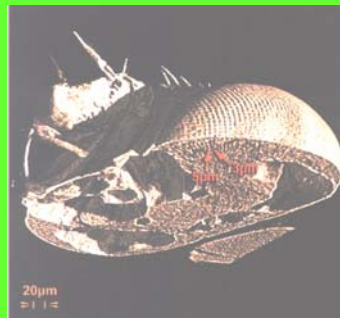
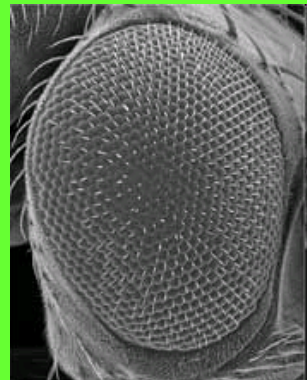
Presented simulation results

- Show that reasonably good directional vision without optics is possible even using the simplest possible detectors whose angular sensitivity is defined only by the surface absorptivity.**
- Are in a good correlation with published observations in studies of cutaneous vision**
- Allow suggesting that the operational principle and capabilities of OLS sensors can be used to model operational principles and capabilities of cutaneous vision and its neural circuitry.**
- Motivate advancing a hypothesis that evolution of vision started from formation, around primordial light sensitive cells, of neural circuitry for implementing imaging algorithms similar to those in our model of the flat OLS sensor, including, at one of the first step, the lateral inhibition.**

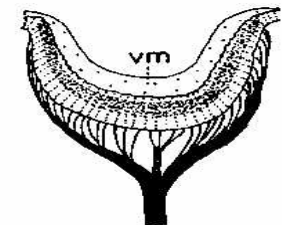
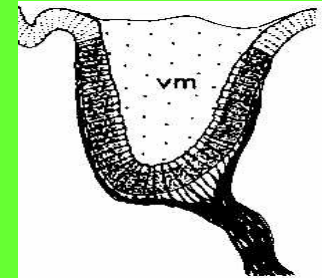
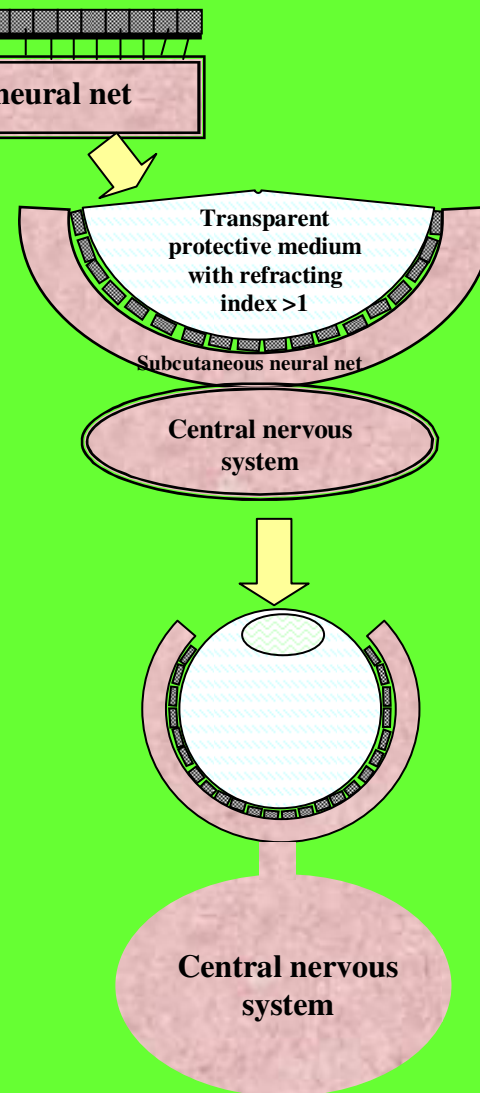
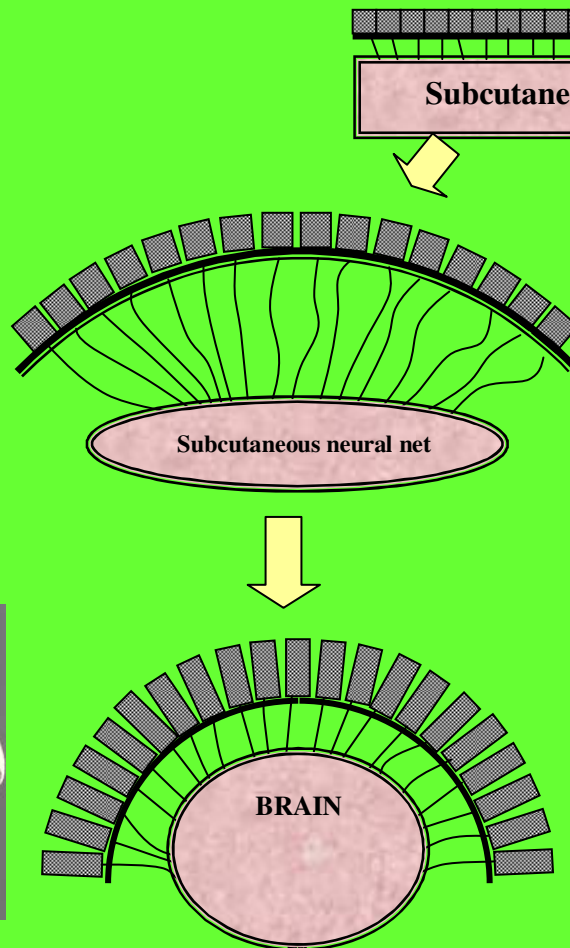
The reported OLS sensor models naturally suggests also, that flat primordial eyespots may have evolved, through bending of the sensor's surface to convex or concave spherical forms, to the compound facet eye or camera-like vision, correspondingly

In both cases, the evolution of eye optics had to be paralleled by the evolution of eye neural circuitry as an inseparable part of animal brains. As it follows from the theory, detection and localization of targets does not necessarily require formation of sharp images and can be carried out directly on not sharply focused images. Image sharpness affects the reliability of detection and becomes important only for low signal-to-noise ratio at detectors. Therefore, gradual improvements of eye optics in course of evolution of eye optics may have translated into improved target detection reliability and allowed transferring, in course of evolution, the higher and higher fraction of eye neural circuitry and brain resources from image formation to image understanding.

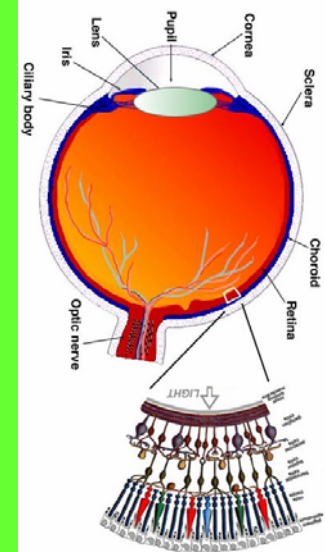
TWO BRANCHES OF EVOLUTION OF VISION



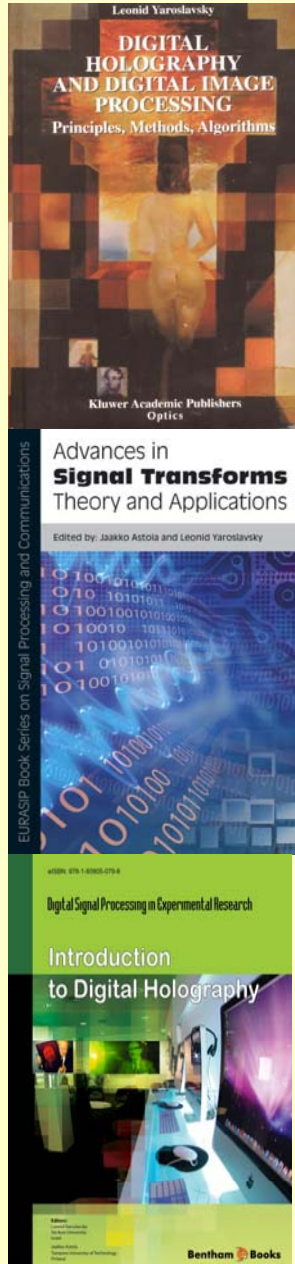
Compound apposition or superposition eyes of insects



Cup eyes of mollusks



Camera like eye of vertebrates



References

1. L. Yaroslavsky, **Digital Holography and Digital Image Processing**, Kluwer Academic Publishers, Optics, Boston, 2004
2. L. Yaroslavsky, **Discrete Transforms, Fast Algorithms and Point Spread Function of Numerical Reconstruction of Digitally Recorded Holograms**, in: **Advances in Signal transforms: Theory and Applications**, J. Astola, L. Yaroslavsky, Eds. , EURASIP Book Series on Signal Processing and Communications, Hindawi, 2007
3. L. Yaroslavsky, **Space Variant and Adaptive Transform Domain Image and Video Restoration Methods**, In: **Advances in Signal transforms: Theory and Applications**, J. Astola, L. Yaroslavsky, Eds. , EURASIP Book Series on Signal Processing and Communications, Hindawi, 2007
4. L. Yaroslavsky, **Fast Discrete Sinc-Interpolation: A Gold Standard for Image Resampling**, In: **Advances in Signal transforms: Theory and Applications**, J. Astola, L. Yaroslavsky, Eds. , EURASIP Book Series on Signal Processing and Communications, Hindawi, 2007
5. L. Yaroslavsky, **Digital Computational Imaging**, In: **Advances in Information Optics and Photonics**, Ari T. Friberg and Rene Daendliker, Eds., SPIE Press, Bellingham, Washington, USA, 2008, pp. 209-227
6. L. Yaroslavsky, **Introduction to Digital Holography**, in: **Bentham Series of e-books “Digital Signal Processing in Experimental Research”**, v. 1., L. Yaroslavsky and J. Astola, Eds., Bentham , 2009



Prof. L. Yaroslavsky
Ph.D., Dr. Sc. Phys&Math

*Dept. of Physical Electronics, School
of Electrical Engineering,
Tel Aviv University,
Tel Aviv, Israel*

Website: www.eng.tau.ac.il/~yaro

E-mail: yaro@eng.tau.ac.il

